

Damage Tolerance of Synthetic-Fiber Mooring Rope: Small-Scale Experiments and Analytical Evaluation of Damaged Subropes and Elements

D. Li, A. Miyase, J. G. Williams, and S. S. Wang

Composites Engineering and Application Center (CEAC)

College of Engineering

University of Houston

Houston, TX 77204-0903

**Final Project Report
Prepared for
Minerals Management Service**

Under the MMS/OTRC Cooperative Research Agreement

**1435-01-99-CA-31003
Task Order 18034
MMS Project Number 472**

September 2002

Abstract

Synthetic-fiber mooring rope is being considered as an important emerging technology for economical petroleum exploration and production from offshore deepwater reservoirs. Polyester mooring ropes have been used successfully for years in Brazil and were recently approved by MMS for use in several MODU drilling operations in the Gulf of Mexico. A critical issue associated with the use of synthetic fiber mooring rope is its damage tolerance of the rope. To address this issue, MMS has initiated several research projects, including the study reported here, to better understand the effect of damage on rope strength and stiffness. In this report, comprehensive small-scale experimental study is presented on both polyester rope elements and subropes containing various degrees of damage in the form of cut yarns or elements. Two types of representative polyester ropes have been investigated in the study. The effects of damage on structural stiffness and mechanical strength of the rope elements and subropes have been determined quantitatively. Based on the established rope mechanics theory, approximate methods of analysis have been introduced to evaluate the residual failure strength of damaged and undamaged rope elements and subropes. The experimental data and analytical results obtained are compared well in all cases studied. The results are expected to serve as a basis for further research into the complex behavior of full-scale ropes with damage by more advanced analytical modeling efforts.

Table of Contents

Abstract	1
1. Introduction	4
2. Objectives	5
3. Materials and Rope Construction	6
3.1 Materials	6
3.2 Rope Elements and Subropes	6
3.2(a) Mooring rope #1	7
3.2(b) Mooring rope #2	7
4. Test Specimens and Sample Preparation	8
4.1 Test Specimens	8
4.1(a) Yarn material and test specimen (Mooring rope #1)	8
4.1(b) Strand material and test specimen (Mooring rope #1)	8
4.1(c) Element material and test specimen (Mooring rope #1 and #2)	8
4.1(d) Subropes and test specimens (Mooring rope #1 and #2)	8
4.2 Data Acquisition and Data Analysis	9
4.3 Preparation of Damaged Rope Element and Subrope Test Specimens	9
5. Experimental Procedure	11
6. Approximate Methods for Evaluation of Failure Strength & Torque of Damaged (and Undamaged) Rope Elements and Subropes	12
6.1 Rope Elements (Mooring rope #1)	12
6.2 Subropes (Mooring rope #1)	14
7. Results and Discussion	16
7.1 Polyester Yarns	16
7.2 Polyester Rope Strands	16
7.3 Polyester Rope Elements without Damage	16
7.4 Polyester Rope Elements with Damage	17
7.5 Polyester Mooring Subropes without Damage	19

7.6 Polyester Mooring Subropes with Damage	19
7.7 Comparison between Analytical Predictions and Experimental Results	20
7.7(a) Predictions of rope element failure	20
(1) Rope element without damage	20
(2) Rope element with damage	21
7.7(b) Predictions of subrope failure	21
8. Summary and Conclusions	23
9. References	24
10. Acknowledgements	25
11. Tables	26
12. Figures	29

1. INTRODUCTION

Recently, a considerable amount of technology development has been made on economical recovery of petroleum resources from deepwater offshore. The definition of deepwater has been expanded in the last decade to now include water depth as great as 10,000 feet and beyond. Many different concepts have been introduced for design and construction deepwater platforms, including FPSO's, SPAR's and TLP's. Each concept makes use of mooring lines or tethers for station keeping. For example, the taut-leg mooring line concept in which multiple light-weight synthetic-fiber ropes, such as polyester ropes, are used and suspended from a platform to the seabed at an angle of approximately 45 degrees from vertical, is an attractive candidate with growing popularity. Petrobras has made a major commitment [1] to this approach with over 1½ dozen platforms so anchored. There has been a considerable amount of interest emerging in using synthetic-fiber mooring ropes in other parts of the world, including the Gulf of Mexico (GOM).

In 2001, the American Petroleum Institute (API) introduced its guidelines [2] for design, manufacturing, installation and maintenance of synthetic fiber mooring ropes. The US Minerals Management Service (MMS) recently approved the use of FPSO systems [3] in the Gulf of Mexico (GOM). Several MODU drilling platforms were given approval to use polyester mooring ropes in the deepwater GOM drilling programs. Among various engineering issues, the MMS has expressed its serious concern with the reliability of synthetic fiber mooring ropes containing damage. Consequently, it has been sponsoring research projects to address the damage tolerance issue of polyester mooring ropes, including a review study on handling & installation damage [4] concerning the following topics:

- (1) Rope handling the rope during installation.
- (2) Wear experienced during service.
- (3) Ingress of sand and marine growth.
- (4) Material & manufacturing defects.
- (5) Local subrope or element rupture during service.

Also, an integrated program which has recently been devised by MMS, including: (1) testing of small-scale rope components, (2) analytical modeling, and (3) large-scale testing program, attempts to address systematically the critical issue of rope damage tolerance. The first item in the list is the focus of the present study. The results obtained from the present study are expected to be used for subsequent validation of an analytical model development. The ultimate goal of the MMS program is to develop guidelines for assessing safety and reliability of damaged mooring ropes.

2. OBJECTIVES

The primary objective of the study is to investigate, with small-scale experiments, the behavior of selected synthetic mooring rope elements and subropes containing different degrees of damage. Specific goals to be accomplished in the project are as follows:

1. Determine quantitatively load-deformation characteristics, structural stiffness, and failure strength of small-scale components - rope elements and subropes - from representative polyester mooring ropes considered for use in offshore production systems.
2. Study experimentally the effects of damage size and mode on stiffness change, local stress concentrations and failure strength degradation of constituent polyester rope elements and subropes.
3. Provide a detailed quantitative database of mechanical strength degradation and stiffness reduction in two types subropes and rope elements with different architectures and construction for the accurate analytical modeling effort conducted elsewhere.
4. Develop approximate methods of analysis, based on the established rope mechanics, to analyze and interpret the present experimental results.

3. MATERIALS AND ROPE CONSTRUCTION

3.1 Materials

Although many fiber manufacturers routinely provide typical yarn properties in the form of product data sheets, rope material constitutive behavior such as its stress-strain relationship, has not been generally available. The tensile stress-strain behavior of a single polyester fiber, for example, a 1000-denier yarn and a 20-ply 1000-denier yarn, has been reported in [5] and [6], respectively. The materials tested were generally in a pristine condition, not taken from a mooring rope. Manufacturing a mooring rope with a complex architecture may introduce damage due to abrasion among the fibers/yarns, leading to degradation of its mechanical properties. Bending a rope in which fibers are laterally constrained can introduce kinking damage. Consequently, the mechanical state and material properties obtained from the fibers and yarns taken from a mooring rope may be different those from their “as manufactured” states.

3.2 Rope Elements and Subropes

The architecture of a candidate mooring rope is primarily one of the following two types, i.e., parallel lay or strand rope construction. A rope with a parallel lay structure may have all fibers or yarns laid parallel to the axis of the rope, or a rope may be composed of multiple subropes that are laid parallel to the axis of the rope. Each subrope is made of a number of elements, which may have a twisted or braided architecture. The rope element is composed of strands, which may also be twisted. The entire assembly of subropes is normally encapsulated in a braided jacket to maintain their integrity. Subropes and rope elements may or may not have a braided jacket, depending on the preference of a manufacturer. Some ropes are now constructed with a filter material inside the rope braid to help prevent ingress of sand particles or mud. Field terminations are primarily of two types, i.e., eye splice and potted, with the eye-splice termination being the most widely used.

The current investigation has been focused on two different designs of parallel-lay polyester fiber mooring ropes described below as Mooring Rope #1 and #2. The laboratory test machines used in the study could not accommodate the long-length specimens with eye-splice type terminations. Thus alternative load-introduction devices were used, including spike-and-cone terminations and potted terminations. For the small-scale test specimens used in this investigation, these terminations were expected to provide failure loads approaching the element and subrope ultimate strengths.

Results given in the present report include test data on yarns, strands, elements and subropes of Mooring Rope #1 and also on elements and subropes of Mooring Rope #2.

3.2(a) Mooring rope #1

Mooring Rope #1 was a parallel-lay polyester fiber rope, comprised of 28 subropes as shown in Fig. 1. Each subrope contained three elements twisted in either a clockwise or counter-clockwise direction. The element had a period of approximately 5.9 inches (150 mm). Each element was constructed from nine strands, each with twenty yarns of 2,000 deniers. The helical strands in each element had a period of approximately 3.2 inches (81 mm). The polyester fibers in the rope were designated as Doilen® 855 TN Oceanic with a marine finish. All strands had a twist in either a clockwise or counter-clockwise direction. (The rope was manufactured by Marlow Ropes. Marlow's data showed that the rope had a strength of approximately 470 kips and a subrope had a strength of approximately 17.3 kips.) The diameter of the rope was approximately 3.3 inches; the subrope approximately 0.55 inch; and the element approximately 0.3 inch. Illustrations of the yarns, strands and elements for Mooring Rope #1 used in the study are given in Fig. 2. A summary of key microstructural parameters of Mooring Rope #1 is shown in Table 1. We note that Mooring Rope #1 is similar to the one used in the DeepStar mooring rope field-test program [8].

3.2(b) Mooring rope #2

Mooring Rope #2 was composed of seven parallel-laid subropes encapsulated in a braided jacket with a braid angle of approximately 65 to 70 degrees, measured from the longitudinal axis of the rope (Fig. 3). The nominal diameter of the rope, including a braided jacket, was approximately 2.9 inches, and the diameter of the subrope was approximately 1 inch. Each subrope was composed of four elements twisted in a right-hand lay, strand-rope type construction around a smaller-diameter, axially-oriented center (core) element. Each element including its jacket had a diameter of approximately 0.41 inch. The pitch length of the elements in a subrope was approximately 4.5 inches. The small central core element was made of polypropylene fibers and had a diameter, including a braided jacket, of approximately 0.25 inch. The subrope was designed to achieve a predetermined torque similar to that for a steel wire rope. Each element in the subrope contained 39 strands of Type 68 DuPont polyester fibers. Each strand had 16 yarns with nominal 2000 yarn denier. The total element cordage was thus approximately 1,248,000 denier. Elements were encapsulated in a braided jacket with a braid angle of approximately 45 degrees relative to the axis of the element. The measured twist period of a yarn within the element was 8.6 inches. A summary of key microstructural parameters of Mooring Rope #2 is shown in Table 2. (The rope was supplied by Whitehill Manufacturing Corporation with designation VETS 351 Great White Rope). Test data on the rope material provided by the manufacturer indicated a tensile strength of approximately 251 kips pounds for the rope, and 39.25 kips for the subrope [9].

4. TEST SPECIMENS AND SAMPLE PREPARATION

4.1 Test Specimens

4.1(a) Yarn material and test specimen (Mooring rope #1)

The polyester yarn size was checked by weighing 20 individual yarns of 12-inch length taken from four different strands of Mooring Rope #1. The average value of the yarns was found to be 2020 deniers with a coefficient of variation of one percent (versus the nominal 2000 denier description by the manufacturer). Little or no twist was observed in the yarns.

Yarn specimens were prepared using a technique similar to the one described in ASTM-D 3379 for a single-filament test [10]. Individual yarns were carefully separated and mounted 1-inch apart on a picture-frame shaped cardboard with a 7-inch long by 8-inch wide opening, using a masking tape. An epoxy adhesive was applied between the yarn and the cardboard to form a 1.5-inch grip region.

4.1(b) Strand material and test specimen (Mooring rope #1)

Polyester strand specimens were made with the same technique as that for the yarn specimens. The original twist was preserved during sample preparation. After the epoxy adhesive was hardened, the cardboard support was cut to make individual strand test specimens. The grip section of the strand specimen was inserted into a 1.5-inch long copper tubing with a 0.25-inch outer diameter. After squeezing the copper tubing end, the gap between the copper tubing and the strand specimen was filled with an epoxy resin.

4.1(c) Element materials and test specimens (Mooring rope #1 and #2)

Rope element test specimens (for both Mooring Rope #1 & #2) were prepared, using a commercially available aluminum cone-and-spike (or barrel-and-spike) type termination, as illustrated in Fig. 4. The element and subrope specimens (of Mooring Rope #1) had a nominal length of 24 inches between end terminations. Preliminary tests indicated a premature failure due to abrasion of the fibers with the aluminum cone and steel spike in the contact area within the grips. This was resolved by inserting a thin piece of paper or tape between the fiber and metal parts. Data recorded included axial loads and strains and, in a limited number of tests, the change of specimen diameter during loading. Rotation of the termination at the end of each test specimen was also measured during the experiment.

4.1(d) Subropes and test specimens (Mooring rope #1 and #2)

Subrope specimens were tested, using a conical-shape metal termination into which fibers were inserted. A room-temperature-cured epoxy potting material was used to bond the polyester fiber subrope (Mooring rope

#1 only) inside the termination (Fig. 5). The elements within the subrope were separated into yarns to achieve maximum resin penetration and adhesion. In the makeup of element and subrope test specimens, the original twist residing in the rope was marked and kept to maintain the original configuration and pitch length of the yarns and the elements.

A special procedure for preparing the subrope test specimens made from Mooring Rope #2 included the following key steps:

- (1) Removal of braided jackets of individual elements and washing out the abrasion-resistant coating on fibers with fresh water (Fig.6).
- (2) After drying fibers, presoaking all fibers by stirring the fibers with a hand tool (Fig. 7).
- (3) Applying heat to improve resin bonding (by wrapping a heating tape on the socket surface) (Fig. 8).

4.2 Data Acquisition and Data Analysis

The data collected in a subrope test included the load-cell response, axial strain, and the change in specimen diameter during loading. Strains were measured with two LVDT's connected to the test specimen by a (polyester) sewing thread secured to the rope using a rubber band. Small pulleys were used to allow the LVDT's to be mounted remote from the rope. This arrangement gave the test specimen a gage length up to 24 inches that would result in high accuracy. Most rope element tests were conducted on specimens with a gage length containing three periods of twist. For the tests involving damaged (cut) strands, the string for both LVDT's was secured to the uncut strands or elements. Torque generated during the test was measured, using a load cell mounted on a lever arm attached to a conical metal fixture at one end and restrained by a test machine column on the other. The test system setup for Mooring Rope #1 is shown in Fig. 9.

The expected higher ultimate failure load of Mooring Rope #2 required the use of a larger capacity test machine as shown in Fig. 10. A built-in load cell automatically recorded the torque generated during the test. The stroke length of the larger test machine limited the maximum subrope test specimen to a gage length of two periods of the twist.

4.3 Preparation of Damaged Rope Element and Subrope Test Specimens

The damage introduced into both element and subrope specimens was made by cutting a predetermined amount of yarns or strands with scissors or a sharp razor blade. The procedure for preparing a damaged specimen from Mooring Rope #1 involved cutting strands in selected elements after the specimen was mounted in the test machine as illustrated in Fig. 11. The procedure for preparing damaged test specimens from Mooring Rope #2 was to place a shrinking tube around the selected element and cut carefully through the tube and the

element to a desired depth as shown in Fig. 12. Proper insulation was placed around the rope element surface during heating the shrink tube to minimize the adverse heating effect. After cutting the element cross section to a prescribed depth, the shrink tube was longitudinally cut to ensure no constraint was left.

5. EXPERIMENTAL PROCEDURE

Tensile tests on the aforementioned yarn, strand, element and subrope specimens were carried out, using a servo-hydraulic material test machine. Flat-face grips were used for the yarn and strand specimens, and clevis and pin arrangements for the element specimens. All tests were conducted under a displacement-controlled tensile loading mode at a strain rate of approximately 4 percent per minute. Strain measurements were made using an extensometer of a 0.5-inch gage length for the yarn and strand test specimens. Another extensometer with a 2-inch gage length and an in-house built LVDT extensometer with a variable gage length up to 24 inches were used for evaluating the rope element and subrope specimens. In selected rope element and subrope tests, an in-house built diametric extensometer was used to measure lateral dimensional changes of the specimens (see Fig. 13). During the tensile tests, force and strain measurements were recorded using a computer-aided data acquisition system. Specimens were tested dry in both dry ambient and as-received conditions without an environment or load preconditioning. The original orientations (twists) of the strand, element or subrope within the rope architecture were maintained when the specimens were mounted in the test system.

The lower piston of the servo-hydraulic test machine had almost negligible resistance to torque. Since the rope elements and subropes were not torque-balanced, specimen rotations occurred during loading and their final rotation angles were recorded. A few subrope tests were also conducted without the torque restraint. However, the rotations were found to be very significant as to interfere with the aforementioned strain measurements. A torque restraint which was incorporated with a load cell was then installed, thus allowing to measure the torque generated during the test (see Fig. 14).

6. APPROXIMATE METHODS FOR EVALUATION OF FAILURE STRENGTH & TORQUE OF DAMAGED (AND UNDATED) ROPE ELEMENTS AND SUBROPES

The detailed architecture of synthetic-fiber mooring ropes introduces significant complexities in micromechanical modeling of deformations and failure of rope elements and subropes. Geometric, material, damage mode and microstructural parameters involved in rope construction need to be included in analytical models. In the absence of such analytical models at present, an approximate micromechanics analysis, based on the existing well-known rope mechanics [13] is introduced for evaluating the current experimental results. The residual failure strength, material deformation, and the torque generated in the damage tolerance tests have been determined with the analysis. Numerical examples are conducted on both damaged and virgin rope elements and subropes of Mooring Rope #1 for illustrative purposes. Comparisons are made between the analytical predictions and the experimental results.

6.1 Rope Elements (Mooring Rope #1)

Each individual rope element was made from a nine-strand construction (in Mooring Rope #1). Also each strand was twisted and had a symmetric geometry in its virgin state. Consider a simple helical strand element shown in Fig. 15, where N_2 and N'_2 are components of the shearing force on an outer strand along X and Y directions; T_2 is the axial tension in the strand; G_2 and G'_2 are components of the bending moment on an outer strand along X and Y directions. H_2 is a twisting moment in the strand; and X_2 is a component of the external line load per unit length along the centerline of the outer strand in the X direction.

Assume that the rope element is under pure tension (no external bending moment) and that the axial tension T_2 is constant along the strand. Then the equations of equilibrium of the strand can be written as [13]

$$-N'_2 \bar{\tau}_2 + T_2 \bar{\kappa}'_2 + X_2 = 0 \quad (1)_a$$

$$-G'_2 \bar{\tau}_2 + H_2 \bar{\kappa}'_2 + N'_2 = 0 \quad (1)_b$$

where κ'_2 is a component of the strand curvature in the Y direction; τ_2 is the twist per unit length of the strand, and the overbar refers to a deformed state.

The helical angle α_2 of an outer strand is determined by the relation, $\tan \alpha_2 = P_2 / 2\pi r_2$, where P_2 is the initial pitch of the outer strand and r_2 is the radius of the helical outer strand (Fig.16). The initial strand curvature and twist per unit length are [13]

$$\kappa'_2 = \cos^2 \alpha / r_2 \quad (2)_a$$

$$\tau_2 = \sin \alpha \cos \alpha / r_2 \quad (2)_b$$

Under loading, the outer helical strand is assumed to deform into a new helical configuration with a new curvature and twist as,

$$\bar{\kappa}'_2 = \cos^2 \bar{\alpha} / \bar{r}_2 \quad (3)_a$$

$$\bar{\tau}_2 = \sin \bar{\alpha} \cos \bar{\alpha} / \bar{r}_2 \quad (3)_b$$

$$|\Delta \alpha_2| = |\bar{\alpha}_2 - \alpha_2| \ll 1 \quad (4)$$

Let ξ_1 be the axial strain in an outer strand (i.e. $\xi_1 = \varepsilon$); ξ_2 , the axial strain in the center strand, and ν , the Poisson's ratio of the strand.

The change in curvature $\Delta \kappa'_2$ and in twist per unit length $\Delta \tau'_2$ can then be linearized as

$$\begin{aligned} R_2 \Delta \kappa'_2 &= \cos^2 \bar{\alpha}_2 (R_2 / \bar{r}_2) - \cos^2 \alpha_2 (R_2 / r_2) \\ &= -2 \sin \alpha_2 \cos \alpha_2 (R_2 / r_2) \Delta \alpha_2 + \nu [(R_1 \xi_1 + R_2 \xi_2) / r_2] \cos^2 \alpha_2 (R_2 / r_2) \end{aligned} \quad (5)_a$$

$$\begin{aligned} R_2 \Delta \tau_2 &= \sin \bar{\alpha}_2 \cos \bar{\alpha}_2 (R_2 / \bar{r}_2) - \sin \alpha_2 \cos \alpha_2 (R_2 / r_2) \\ &= (1 - 2 \sin^2 \alpha_2) (R_2 / r_2) \Delta \alpha_2 + \nu [(R_1 \xi_1 + R_2 \xi_2) / r_2] \sin \alpha_2 \cos \alpha_2 (R_2 / r_2) \end{aligned} \quad (5)_a$$

In the outer strand, considering the load and deformation relation and the equations of equilibrium, one can write the following relationships for the strand under loading.

$$\frac{G'_2}{ER_2^3} = \frac{\pi}{4} R_2 \Delta \kappa' \quad (6)_a$$

$$\frac{H_2}{ER_2^3} = \frac{\pi}{4(1+\nu)} R_2 \Delta \tau_2 \quad (6)_b$$

$$\frac{T_2}{ER_2^3} = \pi \xi_2 \quad (6)_c$$

$$\frac{N'_2}{ER_2^3} = \frac{H_2}{ER_2^3} \frac{\cos^2 \alpha_2}{r_2 / R_2} - \frac{G'_2}{ER_2^3} \frac{\sin \alpha_2 \cos \alpha_2}{r_2 / R_2} \quad (6)_d$$

$$\frac{X_2}{ER_2^3} = \frac{N'_2}{ER_2^3} \frac{\sin \alpha_2 \cos \alpha_2}{r_2 / R_2} - \frac{T_2}{ER_2^3} \frac{\cos^2 \alpha_2}{r_2 / R_2} \quad (6)_e$$

A projection of the force acting on the outer strands in the axial direction yields,

$$\frac{F_2}{ER_2^2} = m_2 \left[\frac{T_2}{ER_2^2} \sin \alpha_2 + \frac{N'_2}{ER_2^2} \cos \alpha_2 \right] \quad (7)$$

where F_2 is the total axial force in the remaining m_2 outer strands. (Note: $m_2 = n - m_1 - 1$, with n = total number of strands per element, and m_1 is the number of cut strands). The total axial twisting moment (i.e., torque) M_2 acting on the remaining m_2 outer strands can be found [13] as

$$\frac{M_2}{ER_2^3} = m_2 \left[\frac{H_2}{ER_2^3} \sin \alpha_2 + \frac{G'_2}{ER_2^3} \cos \alpha_2 + \frac{T_2}{ER_2^2} \frac{r_2}{R_2} \cos \alpha_2 - \frac{N'_2}{ER_2^2} \frac{r_2}{R_2} \sin \alpha_2 \right]. \quad (8)$$

The axial force F_1 and the axial twisting moment (torque) M_1 acting on the center strand are given by:

$$\frac{F_1}{ER_1^2} = \pi \zeta_1 \quad (9)_a$$

$$\frac{M_1}{ER_1^3} = \frac{\pi}{4(1+\nu)} R_1 \tau_s \quad (9)_b$$

The total axial force F and the axial twisting moment (torque) M acting on the element (damaged and undamaged) can then be determined by:

$$F = F_1 + F_2 \quad (10)_a$$

$$M = M_1 + M_2 \quad (10)_b$$

6.2 Subropes (Mooring rope #1)

Each subrope in Mooring Rope #1 consists of three rope elements. These elements were twisted and deformed to into a helical shape. One may establish a similar model for the subrope as that for the rope element. One could also envision a visual element in the center of the subrope and the strains of its center and outer strands being ξ_1 and ξ_2 . (Note ξ_1 is equal to the strain of the subrope). Denote ξ_3 as the strain in the center strand and ξ_4 , in an outer strand of an outer element. Let the helical angle of the subrope be α^*_2 . As the subrope is loaded, its helical angle now assumes a new $\bar{\alpha}^*_2$. The angle of twist per unit length of the subrope becomes

$$\Delta^* \tau_2 = (\sin \bar{\alpha}^*_2 \cos^* \bar{\alpha}_2 / \bar{r}^*_2) - (\sin \bar{\alpha}^*_2 \cos^* \bar{\alpha}_2 / r^*_2), \quad (11)_a$$

in which the r^*_2 (Fig.20) has the value,

$$r^*_2 = (2/\sqrt{3}) * (2R_4 + R_3). \quad (11)_b$$

Due to Poisson's effect, one has

$$\bar{r}^*_2 = r^*_2 - \nu(2R_4\xi_4 + R_3\xi_3), \quad (11)_c$$

where R_3 and R_4 are shown in Fig. 20.

The helical angle α^*_2 of an outer rope element can be determined by the relation,

$$\tan \alpha^*_2 = \bar{P}^*_2 / 2\pi r^*_2 \quad (11)_d$$

where \bar{P}^*_2 is the initial pitch of the outer element.

Following the same approach as that for the rope element analysis, the following equilibrium equations can be introduced [13] for the subrope:

$$\xi_3 = \xi_4 + \frac{\Delta \alpha_4}{\tan \alpha_4} \quad (12)_a$$

$$r_2^* \tau = \frac{\xi_3}{\tan \alpha_2^*} - \Delta \alpha_2^* + \frac{\nu}{r_2^*} \frac{(2/\sqrt{3}) * (2R_4 + R_3)}{\tan \alpha_2^*} \quad (12)_b$$

$$\begin{aligned} (R_3 + R_4) \Delta \tau_2^* &= \frac{\xi_4}{\tan \alpha_4} - \Delta \alpha_4 + \nu \frac{(R_4 \xi_4 + R_3 \xi_3)}{(R_4 + R_3) \tan \alpha_4} \\ &= \frac{(R_4 + R_3)}{r_2^*} \left[(1 - 2 \sin^2 \alpha_2^*) \Delta \alpha_2^* + \nu (2/\sqrt{3}) \frac{(2R_4 \xi_4 + R_3 \xi_3)}{r_2^*} \sin \alpha_2^* \cos \alpha_2^* \right] \end{aligned} \quad (12)_c$$

where $\Delta \alpha_2^*$, $\Delta \alpha_4$ and ξ_4 are unknowns quantities to be determined from the equations, and $\alpha_4 = \alpha_2$ in the subrope case.

Consider a subrope without damage, the above equations can be easily solved for the three unknowns.

For Mooring Rope #1, one can get

$$\Delta \alpha_2^* = 0.0235, \Delta \alpha_4 = 0.0326 \text{ and } \xi_4 = 0.1233. \quad (13)$$

Once ξ_3 and $\Delta \tau_2^*$ are known, the total twisting moment (torque) H_2^* in the subrope can be determined by:

$$H_2^* = [\pi E / 4(1 + \nu)] (R_3 + R_4)^2 \Delta \tau_2^* \quad (14)_a$$

The bending moment G_2^* in the subrope is then determined by the expression [13],

$$G_2^* = A_2^* [(\cos^* \bar{\alpha}_2)^2 / \bar{r}_2^* - (\cos^* \alpha_2)^2 / r_2^*] \quad (14)_b$$

where A_2^* is the total bending stiffness of outer elements with

$$A_2^* = 8(\pi E R_4^4 / 4) [2 \sin \alpha_4 / (2 + \nu \cos^2 \alpha_4)] + \pi E R_3^4 / 4 \quad (14)_c$$

The value of N_2^* can be found by the following expression [13]:

$$N_2^* = H_2^* (\cos^* \alpha_2)^2 / r_2^* - G_2^* (\sin^* \alpha_2 \cos^* \alpha_2) / r_2^* \quad (14)_d$$

Thus the total axial force and total axial twisting moment (torque) acting on the subrope may be determined by:

$$F = F_2^* = 3(T_2^* \sin \alpha_2^* + N_2^* \cos \alpha_2^*) \quad (15)_a$$

$$M = M_2^* = 3[H_2^* \sin \alpha_2^* + G_2^* \cos \alpha_2^* + T_2^* r_2 \cos \alpha_2^* - N_2^* r_2 \sin \alpha_2^*] \quad (15)_b$$

7. RESULTS AND DISCUSSION

7.1 Polyester Yarns

The stress-strain relationship of 2000-denier yarns of Mooring Rope #1 has been determined and shown in Fig. 21. The initial slope of the σ - ϵ curve decreased slightly with increasing strain and then increased gradually prior to its final failure. The stress-strain behavior of the yarns taken from different strands shows similar characteristics in deformation and failure strength (Fig. 21). Progressive failure of individual fibers within the yarns was observed during the load increase.

The stress-strain curve of the Mooring Rope #1 yarn is compared (Fig. 22) with that of a 1000-denier ENKA 855TN yarn reported in Ref. [4]. Although the overall deformation behavior of the Mooring Rope #1 yarn is similar to that of the ENKA 855TN yarn, noticeable differences in failure strain and strength can be observed.

7.2 Polyester Rope Strands

The stress-strain behavior of polyester rope strands (Mooring Rope #1) has also been determined and shown in Fig. 23. The initial sigmoidal part may be attributed to kinematic deformation of twist of the strand specimen, and its σ - ϵ relationship follows a similar behavior as that of a yarn. Variations in the stress-strain curves of the strands were more appreciable than those of the yarns because of the strand twist kinematics and other initial geometrically induced initial strains. Progressive failure in the polyester strands during testing was also observed in the gage section as shown in Fig. 24.

Since the strand specimen had a relatively long twisted pitch length, the effect of gage length on strain measurements was checked first. Strain measurements taken from an extensometer over a 2-inch gage length and a LVDT over a 16-inch length in the strand specimens were compared and shown in Fig. 25. Despite the difference in the number of pitches covered by the two distinct measurement devices, the measured strains were in good agreement.

7.3 Polyester Rope Elements without Damage

Tensile test results obtained from undamaged polyester rope elements (Mooring Rope #1) are shown in Figs. 26 and 27. The ultimate strength of the rope element has been determined and given in Tables 3 and 4. General characteristics of the element load-strain behavior were found to be similar to those of the strands. The initial sigmoid and subsequent deformations in the σ - ϵ curve of the rope element were more pronounced due to the kinematics of twist within an element than those in a strand. Significant variations in the element test data were attributed to the difference in the initial amount of twist and to a lesser degree, uneven loading on the strands due to unequal length of the strands unintentionally introduced during specimen preparation. A small

variation in the rope element failure strength was found in the cases which had the failure occurring in the gage region. The characteristic failure mode observed in the undamaged Mooring Rope #1 elements is shown in Fig. 28. Progressive strand failure was found within both the rope element specimen and its terminations.

The tensile stress-strain and load-deformation behavior of undamaged polyester rope elements (Mooring Rope #2) are shown in Figs. 29, 30. Also shown in Fig. 29 are the yarn data provided by the manufacturer. The difference in stiffness was caused by kinematic deformations due to initial element in twist and perhaps some other misalignments. The responses for all, but two, specimens fell in a fairly narrow range. The ultimate strength of the Mooring Rope #2 element measured in the tests is presented in Table 6. Measurements of lateral contraction in an undamaged rope element test as a function of the applied axial strain were made and shown in Fig. 31. A clip-on diametric extensometer was attached on the rope element during the test. Due to Poisson's effect, the cross section of the element specimen contracted under an applied tensile load. The rope element cross-sectional geometry changed axisymmetrically with an increasing axial load. (A discontinuity in the diametric change shown in the figure might be caused by relative movements at the contact point between the specimen and the extensometer contact arm, due to a rotation of the specimen.)

Comparisons among typical stress-strain curves of undamaged polyester yarns, strands and elements are given in Fig. 32. While initial deformation characteristics were similar at the three levels of the rope scale, appreciable differences in strain-hardening at a higher stress could be seen. Their failure strengths are found to be also dependent on the specimen size. The yarns had the highest failure strength and the strand strength was lower than that of the yarns. The rope element strength was lower than both the yarn and the strand strength. With an increasing specimen size, it became difficult to load all fibers uniformly. Therefore, it is possible that fiber-stress variations in a rope element could be largest and the progressive fiber breakage commenced at a lower applied load. The rope element also experienced a high degree of geometrically nonlinear deformation due to twisting kinematics in rope elements, leading to low strain hardening and strength.

7.4 Polyester Rope Elements with Damage

In a damaged rope element specimen, local stress and deformation were not uniformly distributed in the gage section due to the cut introduced. In the absence of a micromechanics description of the local stress concentration near the cut, the damage-tolerance test results of a rope element are expressed in terms of the average local element stress at the cross section containing the cut, $\sigma_n = P / A^*$, where A^* is the net element sectional area and the average strain, $\bar{\epsilon}$, along the gage section. The $\sigma_n - \bar{\epsilon}$ relations for the element tests (Mooring Rope #1) with 1, 3, and 5 strands cut have been obtained and shown in Figs. 33 to 38. Comparison of the element load-strain relationships of the damaged and the undamaged rope elements is given Fig. 39. Ultimate failure strengths of the damaged rope elements are summarized in Tables 3 and 4.

The architecture of the rope element (in Mooring Rope #1) was that one strand was centrally located and surrounded by eight other strands. The test data included several kinds of damage (cutting), both symmetric and asymmetric. An appreciable difference is observed between the results of symmetric and asymmetric damage of the same number of strands, as indicated in Tables 3 and 4. Failure loads of the rope elements with asymmetric cuts were lower than those with symmetric cuts (with same degree of damage). Eccentric deformations caused by an asymmetric cut obviously made load transfer and distribution difficult and nonuniform in the spike and cone termination, resulting in premature failure. Other microstructural factors such as differences in twist of strands, misalignment and slippage of fibers within the termination would all affect the $\sigma_n - \bar{\epsilon}$ response. (Considering the number of the complicated factors involved, the current scatter in the $\sigma_n - \bar{\epsilon}$ behavior appeared to be reasonably bounded.) The strand cut in the center of a rope element allowed other strands to deform freely along the axial (longitudinal) direction as the specimen was loaded (as shown in the two photographs of Fig. 40 taken before and during loading). The cut strands were also relatively slack at the entry into the terminations and thus did not result in sufficient lateral traction to cause load-sharing and transfer. Therefore, the influence of strand damage in this case could be related to a net-area effect in the rope element. Even though some variations have been found in the $\sigma_n - \bar{\epsilon}$ response from test to test, basic characteristics of the $\sigma_n - \bar{\epsilon}$ relationships with and without the strand damage seemed to validate this hypothesis.

Test data of damaged rope elements (Mooring Rope #2) with approximately 15 and 50 percent reduction of cross-sectional area are presented in Figs. 41 and 42. Detailed examinations of the test specimens following their failure, such as the one shown in Fig. 43, enabled to affirm accurately the amount of cross-sectional area loss. Most of the $\sigma_n - \bar{\epsilon}$ results fell within the upper undamaged band; however, the responses of four specimens (i.e., 2 undamaged and 2 damaged) were in the lower band. Discussions with the rope manufacturer revealed no apparent reasons for the two distinct responses of the elements from Mooring Rope #2, as all rope elements used in the study were made in a single run to make subropes.

Examination of the fibers within the untested rope elements revealed a considerable amount of yarn kinking existed as shown in Fig. 44. The yarn kinks seemed to be imposed by bending the rope as evidenced by the predominance of the kinks on one side of the rope section. Rope twists could distribute the kinks to all fibers at different locations along the rope axis.

Relatively high failure strengths of the damaged rope elements were obtained in these tests; however, the element failure almost always involved some influence of the termination. Although some yarns failed within the test section as the load approached its failure strength, other yarns would begin to fail progressively in the termination. During the test, cut ends were often observed to translate as a unit within the braided jacket as indicated by necking down in an element cross-section (Fig. 45). The loose condition of cut ligaments at the

entry to end fittings also indicated that essentially very little load was transferred through shear near the damage region.

7.5 Polyester Mooring Subropes without Damage

The load-deformation response of an undamaged subrope (Mooring Rope #1) is presented in Figs. 46 and 47 with its ultimate failure strength given in Table 5. Four different specimens in the tests exhibited almost identical responses.

The load-deformation response of undamaged subropes (Mooring Rope #2) is presented in Figs. 48 and 49, and their ultimate strengths are given in Table 7. All the three test specimens exhibited premature failure near their terminations. The results also show that the present socket termination was not 100-percent efficient. The failure strength of the subrope obtained here about is 64% of the reported ultimate break load of the subrope, which is close to the value expected by a state-of-the-art approach (Page 17 in [6]) (The strength of socket termination can be as low as 70% of that with a spliced termination.)

7.6 Polyester Mooring Subropes with Damage

Following the same approach in describing the responses of damaged rope elements (Sec. 7.4), the behavior of subrope specimens (Mooring Rope #1) with 5, 9, and 13 strands cut is shown in Figs. 50-55. The measured failure strengths of the damaged subropes are given in Table 5. With the data obtained, it appears that the trend of damaged rope response was similar to that without damage. Considering all the microstructural and geometric variables that may affect the subrope response, the data seem to suggest the damaged subrope failure (Mooring Rope #1) was governed by a net-area response.

While the subrope test to some extent was influenced by the efficiency of the termination, it did, in many cases, also contain material failure in the gage section. A photograph of a damaged subrope failure with 9 strands cut (5 in one element and 4 in the others) is shown in Fig. 56. The failure involved separation of the remaining 4 strands in the element with 5 cut strands and additional damage in the other elements. An interesting phenomenon observed in many tests was local melting of polyester fibers in the vicinity of the breaks and even bonding to adjacent strands away from the break, as shown in Fig. 57. Apparently, the friction generated at failure when fibers sliding relative to one another and the strain energy released were sufficient to melt the fibers.

The results of subrope test specimens (Mooring Rope #2) with 1, 2, and 3 elements cut have been determined and shown in Figs. 58-63. The failure strengths of damaged and undamaged subropes are reported in Table 7. Premature failures were observed in all tests. Load dropping appeared in the experiments due to cone bedding and sliding in the socket except the case of one-element cut. Damage tolerance responses of the

subropes are given in Fig. 64. Failure strength degradation in the damaged subrope tests is shown in Fig. 65. The failure stress is noted to be about the same when a small amount of damage was present and increases when a large amount of damage was introduced in the subrope.

Several experiments on the subropes of Mooring Rope #1 were conducted first without a torque restraint. A torque measurement device was then installed to provide accurate torque measurements in the tests on both undamaged and damaged subrope specimens. The results are given in Fig. 66. The torque generated was found to be approximately linear with the applied load (or strain). The maximum torque measured was approximately 350 in-lbs. Specimens with 9 or 13 cut strands have fairly consistent responses in the tests while more variations were seen in the undamaged subrope and the damaged specimens with 5 strands cut. The torques measured from both undamaged and damaged subrope (of Mooring Rope #2) tests are also given (Fig. 67). A correlation between the maximum torque generated and the failure load was not found in the study.

The lateral contraction of subrope diameter during the subrope test was measured as a function of the applied axial strain (Fig. 68). After an initial deformation at a low load, the subrope diameter reduction increased approximately linearly with the applied load.

7.7 Comparison between Analytical Predictions and Experimental Results

7.7(a) Predictions of rope element failure

In order to evaluate the failure strength of a rope element, one must first establish a rope element failure criterion. In this study, the following criterion is used: A rope element will reach its ultimate strength when the first strand reaches its failure strain ε_f . (Here $\varepsilon_f = 0.128$ was determined from the experimental data from the aforementioned strand tests). Other geometric parameters and material properties used in the failure evaluation are:

- Fiber strands are of circular shape with $R_1 = R_2 = 0.04$.
- The strand is elastic with $E = 1.0 \times 10^6 \text{ psi}$ (from the strand test).
- Poisson ratio is 0.25.

(1) Rope element strength without damage

A rope element reaches its failure strength when its extensional strain reaches the critical ε_f .

Letting $\xi_1 = 0.128$ with outer strands not being restrained from rotation, one may follow [13] to have

$$\xi_2 + \Delta\alpha_2 / \tan \alpha_2 = 0.128, \quad (16)_a$$

$$\xi_2 / \tan \alpha_2 - \Delta\alpha_2 + \nu(R_1\xi_1 + R_2\xi_2) / (r_2 \tan \alpha_2) = 0. \quad (16)_b$$

The system of equations shown above has the solutions as

$$\xi_2 = 0.125 \text{ and } \Delta\alpha_2 = 0.0209. \quad (17)$$

The rope element failure load can be determined by calculating its center strand ultimate load ($F_1 = 643.4$ lb) and the outer strand failure load ($F_2 = 4975.3$ lb),

$$F = F_1 + F_2 = 5619 \text{ lb} \quad (18)_a$$

The total axial twisting moment (torque) M acting on the rope element can also be determined as

$$M = M_2 = 54.4 \text{ in-lb.} \quad (18)_b$$

where the axial twisting torque generated in the center strand is ignored.

(2) Rope element strength with damage

Since fiber strands in a rope element cannot maintain a uniform deformation in an asymmetric configuration, which will lead to a number of additional complexities. Thus the current effort is limited only to symmetric damage cases. Several different types of damage (cut) are illustrated in Figs. 17, 18 and 19. Consider the case of a rope element with a center strand cut. In this case, only outer strands are assumed to take the axial load in the cut section. At some distance away from the cut section, friction between the center and outer strands will pick up the load released by the center strand. The outer strands can extend continually from $\xi_2 = 0.125$ to $\xi_{2f} = 0.128$. Thus the failure load will be $F = F_2 = 5095$ lb. (See Table 3)

With the same approach and considering the case of a rope element with 3 symmetric strands cuts (type D), the failure load is then found to be $F = F_2 = 3821$ lb. In the case of an element with 5 symmetric cuts (type G), the failure load is obtained as $F = F_2 = 2548$ lb. (See Table 3)

The residual failure strength determined by the aftermentional rope mechanics analysis and the tests results obtained from the rope element experiments (for Mooring Rope #1) are given Fig. 69. It can be seen that the results agreed well for both the undamage case and the cases with small damage. For example, only a 0.12% difference exists in case of a rope element with one strand cut. For the elements with small damage, a small difference between predicted and test failure strength is observed. In the case with 5 strands cut, the prediction has a 16% difference from the test results. From the comparison, one can see a noticeable difference when the element rope had a large induced damage.

7.7(b) Predictions of subrope failure

For an undamaged subrope (Mooring rope #1) considered in the study, one can find that the failure load

and the total axial twisting moment (torque) acting on the subrope are

$$F = 16.4 \text{ kips}, \quad (19)_a$$

$$M = -941.4 \text{ lb-in.} \quad (19)_b$$

A comparison between the predicted subrope failure strength and the subrope test data is given in Fig. 47 and in Table 5. The failure strength and the torque generated in a subrope without damage (Mooring Rope #1) are predictable, based on the current rope mechanics analysis. It can be seen that the predicted subrope failure strength is quite close to the test data; however, the maximum torque calculated is larger than that obtained in the tests. One may expect some discrepancies between the test data and the subrope predictions, for the section shape of the subrope under loading would no longer keep its circular geometry as originally assumed in the analysis. The pitch radius of the helical subrope will be reduced more significantly than the deformation assumption made in the rope mechanics formulation. Viscoelastic relaxation is not considered in the present polyester subrope failure analysis.

From the experimental observations in both rope element and subrope tests, the physical deformation mechanisms, viscoelastic material constitutive equations, and multi-scale (strand/element/subrope) interactions are not included in the current rope mechanics model. Thus the suitability and applicability of the existing rope mechanics theory to the damage tolerance problems at and beyond the polyester subrope level remain to be challenged. Also additional variables, such as termination, distribution of damage, nonlinear deformation of the rope element and subrope, etc., are all involved during failure but not considered. The approximate failure strength evaluation of damaged rope elements and subropes here is only a preliminary attempt in this regard.

8. SUMMARY AND CONCLUSIONS

A combined experimental and analytical study has been conducted on rope elements and subropes of two typical polyester mooring ropes. The results obtained here could serve as a useful basis for validation of more advanced analytical models being conducted elsewhere.

We note that the limited traverse distance between crossheads of the test machine available for this study necessitated the use of the spike and cone or potted termination. Using these types of terminations and with careful specimen preparation and handling, one could achieve reasonably consistent results from the small-scale rope element and subrope tests. However, some reductions in ultimate strength are expected using any termination concept, including the eye termination typically used in field installation of large ropes.

The architecture of the ropes used in the study was complex. Any experimental study would be impacted by a subtle change in the rope geometry introduced by handling and inefficiency of terminations. Given the various geometric and material variables of rope elements and subropes, the test results were considered to be relatively consistent. The highest strength values achieved are probably more representative and higher values may still be possible with better terminations and refined procedures.

In the subrope tests (of Mooring Rope #2) with a socket termination, the failure was always found to be close to the narrow end of the resin cone, due to difficulties in achieving good fiber-resin wetting when the encapsulating resin was introduced. In addition, the test machine stroke length limited the maximum specimen length, causing inefficiencies in reaching the ultimate break strength of the specimen.

The similarity of the load-deformation data obtained from the damage tolerance tests indicates that the fundamental nature of the damaged rope elements and subropes is mostly governed by the net-area of the rope material with minor influence caused by fibers misalignment. The lateral constraints introduced during the tests on the damaged yarns, strands, elements and subropes were minimal. Therefore, little load transfer took place in the cut ligaments.

From the present study, one should not conclude that the same response would occur when rope elements and subropes are in a large-size mooring rope, particularly in the interior of a large mooring rope. In this case, one would expect that a considerable amount of lateral constraint could be generated in the interior of the rope and cause significant load redistribution and transfer. The load transfer efficiency and effectiveness in a full-size damaged rope may increase the rope stiffness and damage tolerance.

The analytical modeling of damaged rope elements and subropes, based on established rope mechanics, provides a first-order approximate description of load transfer and micromechanics if the small-scale test samples. The predicted strength reductions in the test specimens are compared well with experimental data.

9. REFERENCES

1. Del Vecchio, C., Costa, L. C. S., and Meniconi, L. C.: “Petrobras Experiences With Deep Water Polyester Moorings”, *Composite Materials for Offshore Operations – 3*, S. S. Wang, J. G. Williams, and K. H. Lo, Eds., University of Houston – CEAC, Houston, TX, 2001, pp. 495-502.
2. API RP 2SM, *Recommended Practice for Design, Manufacture, Installation, and Maintenance of Synthetic Fiber Ropes for Offshore Moorings*, First Edition, American Petroleum Institute, Washington, D.C., March 2001.
3. *U.S. Federal Register*. December 31, 2001.
4. Ayres, R.: “Characterizing Polyester Rope Mooring Installation Damage”, *Technical Report to U.S. Minerals Management Service*, Stress Engineering Services, Houston, TX, November 2001.
5. Backer, S., Seo, M.H., Wu, H.C., and Misra, L.: “Fiber and Yarn Properties as Related to Rope Development in Deep Sea Mooring”, *MIT Sea Grant College Program Final Report*, Technical Report # MITSG 91-26, MIT, Cambridge, MA, 1991.
6. UK Health & Safety Executive, “*Review of Fiber Rope for Offshore Mooring Applications*”, *Offshore Technology Report –OTO 1999 005*, National Engineering Laboratory, London, U.K., April 1999.
7. Mandell, J.F., Steckel, M.G., Chung, S.S., and Kenney, M.C., “Fatigue and Environmental Resistance of Polyester and Nylon Fibers”, *Polymer Engineering and Science*, Vol.27, No.15, 1987, pp.1121-1127.
8. Devlin, P., Flory, J., Fulton, T., and Homer, S., “DeepStar’s Polyester Taut Leg Mooring System Test”, *Proceedings of the Ninth International Offshore and Polar Engineering Conference*, ISOPE, Brest, France, June, 1999.
9. Huntley, M., Veselis, T., and Whitehill, S. S., “Technical Assurance Testing of Polyester Rope for Deep Ocean Mooring Lines”, *Proceedings of the 10th Offshore Symposium*, Houston, Texas, February 20, 2001.
10. Annual Book of ASTM Standard, *Standard Test Method for Tensile Strength and Young’s Modulus for High-Modulus Single-Filament Materials*, ASTM D 3379, American Society for Testing and Materials, Vol.15.3, 1995, pp. 127-130.
11. UK Health & Safety Executive, “Resin-Socket Termination of Offshore Strand Ropes”, *Offshore Technology Report-OTO 2000 069*, National Engineering Laboratory, London, U.K., Sep., 2000.
12. McKenna, H.A., “Mooring Line Termination Technology”, *Sea Technology*, Vol. 37, July, 1996, pp.15-18.
13. Costello, G.A., *Theory of Wire Rope*, Springer-Verlag, New York, NY, 1990.

10. Acknowledgements

The authors wish to express their appreciation to the U.S. Minerals Management Service (MMS) for sponsoring this research, and to Acordis Industrial Fibers, Marlow Ropes, and Whitehill Manufacturing Corporation for providing test materials. The discussion with and encouragement from Dr. Charles Smith of MMS are also acknowledged.

11. TABLES

Manufacturer	Mooring Rope #1 (Marlow Ropes)
Diameter of Rope	3.3 inch
Numbers of subropes per rope	28
Diameter of subrope	0.55 inch
Number of elements per subrope	3
Diameter of element	0.3 inch
Pitch of element	5.9 inch
Number of strands per element	9
Diameter of strand	0.08 inch
Pitch of strand	3.2 inch

Table 1 Geometric and microstructural parameters of Mooring Rope #1

Manufacturer	Mooring Rope #2 (Whitehill Ropes)
Diameter of Rope	2.9 inch
Number of subropes per rope	7
Diameter of subrope	1 inch
Number of elements per subrope	4
Diameter of element	0.41 inch
Diameter of core element	0.25 inch
Pitch of element	4.5 inch
Number of strands per element	39
Diameter of strand	0.07 inch*
Pitch of strand	8.6

*Calculated from average one strand occupied area in element

Table 2 Geometric and microstructural parameters of Mooring Rope #2

Test Condition (Symmetric damage)	Number of Tests	Failure Load (kip)		Failure Stress (ksi) (σ_f or σ_{nf})	Failure Strain (%) (ε_f or $\bar{\varepsilon}_f$)	Rotation Angle (degree)
		Test	Prediction			
Undamaged	3	5.03~5.77	5.62	111.52~ 127.99	12.2~13.5	15~25
1 strand Cut	3	5.02~5.18	5.10	125.65~129.38	10.4~13.8	13~16
3 Strands Cut	6	3.01~3.83	3.82	100.33~127.60	10.6~13.2	2~18
5 Strands Cut	6	1.79~2.24	2.55	89.55~112.33	11.0~15.9	N/A

**Table 3 Test data from rope element experiments and analytical predictions
(Mooring Rope #1, symmetric cut).**

Test Condition (Non-symmetric damage)	Number of Tests	Failure Load (kip)	Failure Stress (ksi) (σ_f or σ_{nf})	Failure Strain (%) (ε_f or $\bar{\varepsilon}_f$)	Rotation Angle (degree)
Undamaged	3	5.03~5.77	111.52~ 127.99	12.2~13.5	15~25
1 strand Cut	3	4.41~4.60	110.25~114.82	12.7~12.8	15~17
3 Strands Cut	3	2.22~2.59	71.93~87.00	7.8~11.6	5~9
5 Strands Cut	3	1.39~1.53	69.44~76.60	9.20~10.6	N/A

Table 4 Test data from rope element experiments (Mooring Rope #1, non-symmetric cut).

Test Condition	Number of Tests	Failure Load (kip)	Failure Stress (ksi) (σ_f or σ_{nf})	Failure Strain (%) (ε_f or $\bar{\varepsilon}_f$)	Maximum Torque (lb-inch)
Undamaged	3	10.23~15.4*	75.84~114.05	10.3~13.8	189.6~342.0
5 Strands Cut	3	11.42~13.44	104.0~122.2	13.5~15.4	129.53~253.2
9 Strands Cut	3	10.95~11.08	121.7~122.74	13.3~15.8	291.6~360.7
13 Strands Cut	3	7.1~9.27	101.49~132.53	16.1~16.5	97.9~126.43

*Prediction: $F = 16.4$ kips and $M = -0.94$ kips -in.

Table 5 Test data from subrope experiments and analytical predictions (Mooring Rope #1).

Test Condition	Number of Tests	Failure Load (kip)	Failure Stress (ksi) (σ_f or σ_{nf})	Failure Strain (%) (ε_f or $\bar{\varepsilon}_f$)
Undamaged	8	5.35~8.50	68.68~109.14	10.9~11.9
15% Cross-Sectional Area Reduction	3	6.58~7.19	103.57~108.5	11.7~12.8
50% Cross-Sectional Area Reduction	4	3.81~4.73	88.33~115.87	10.7~15.5

Table 6 Test data from rope element experiments (Mooring Rope #2).

Test Condition	Number of Tests	Failure Load (kip)	Failure Stress (ksi) (σ_f or σ_{nf})	Failure Strain (%) (ε_f or $\bar{\varepsilon}_f$)	Maximum Torque (kip-inch)
Undamaged	3	22.14~24.67	70.96~79.07	14.1~16.2	1.31~3.31
1 element Cut	3	15.32~17.62	63.92~73.43	13.6~19.4	0.72~0.93
2 elements Cut	3	12.64~14.47	80.00~91.60	12.6~17.0	0.24~0.47

3 elements Cut	2	6.34~7.24	81.36~93.02	14.3~15.7	0.02~0.08
----------------	---	-----------	-------------	-----------	-----------

Table 7 Test data from subrope experiments (Mooring Rope #2).

12. FIGURES



Figure 1 Mooring rope #1.



Figure 2 Definitions of strand, element and subrope (Mooring rope #1).

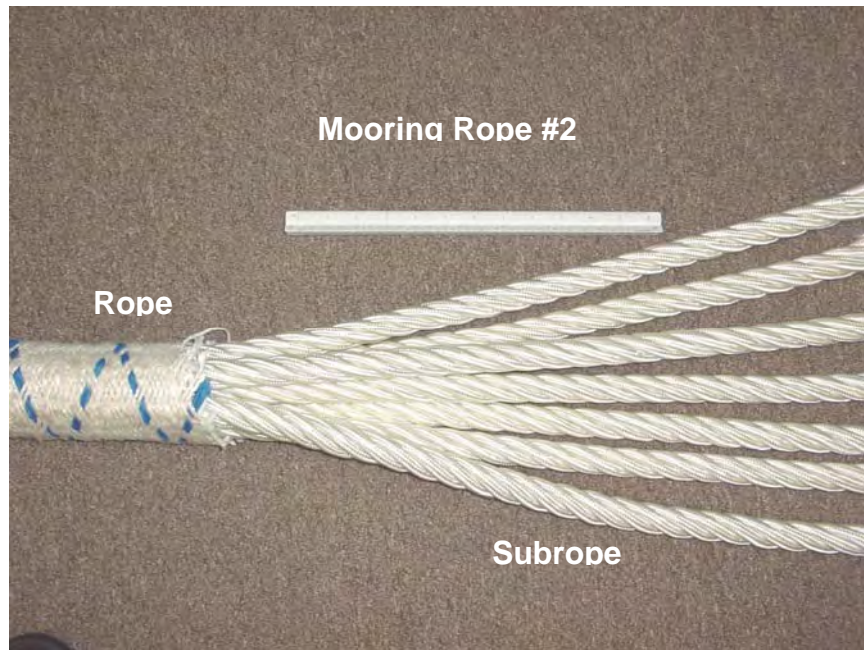


Figure 3 Mooring rope #2 construction.



Figure 4 Spike and cone termination.



(a) Fiber strands in the cone. (b) Epoxy potting.

Figure 5 Potting subrope test specimen (Mooring rope #1).



Figure 6 Rope with braided jacket removed (Mooring rope #2).



Figure 7 Pre-soaking brush fibers of a subrope specimen (Mooring rope #2).



Figure 8 Curing resin inside socket with a heating tape (Mooring rope #2).



Figure 9 Experimental facilities and setup for subrope test (Mooring Rope #1).



Figure 10 – Subrope test with end termination fixed in test machine (Mooring rope #2).



Figure 11 A subrope with damage (cut) (Mooring rope #1).

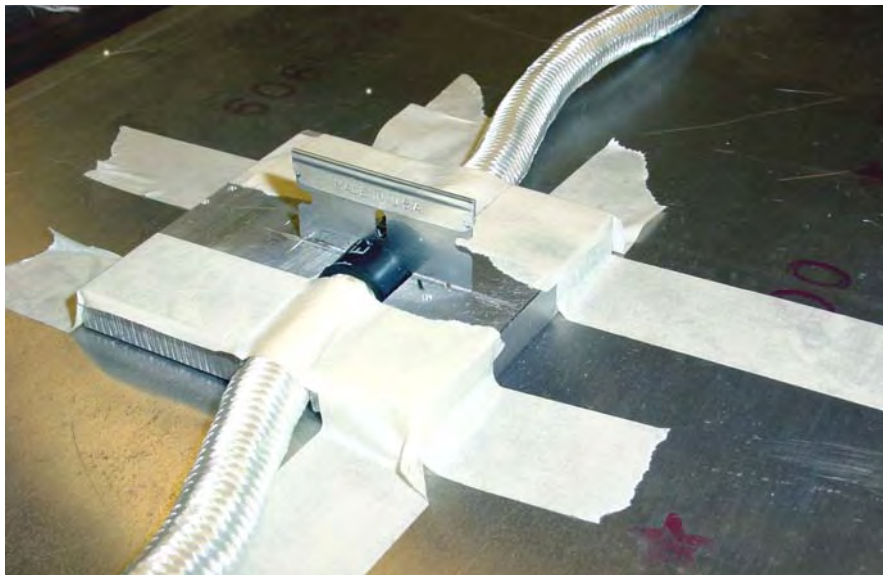


Figure 12 A rope element with damage (cut) (Mooring rope #2).

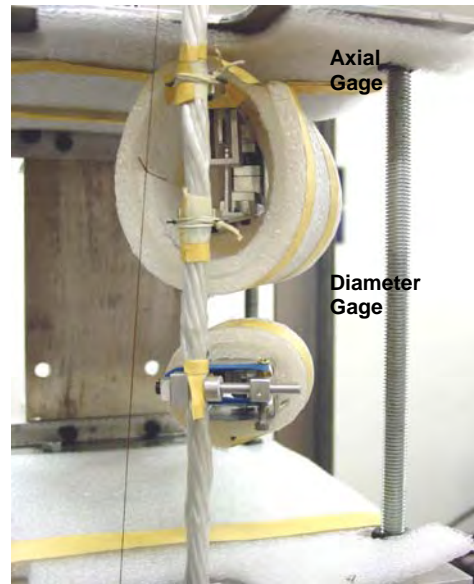


Figure 13 Extensometers for axial and lateral deformation measurements.

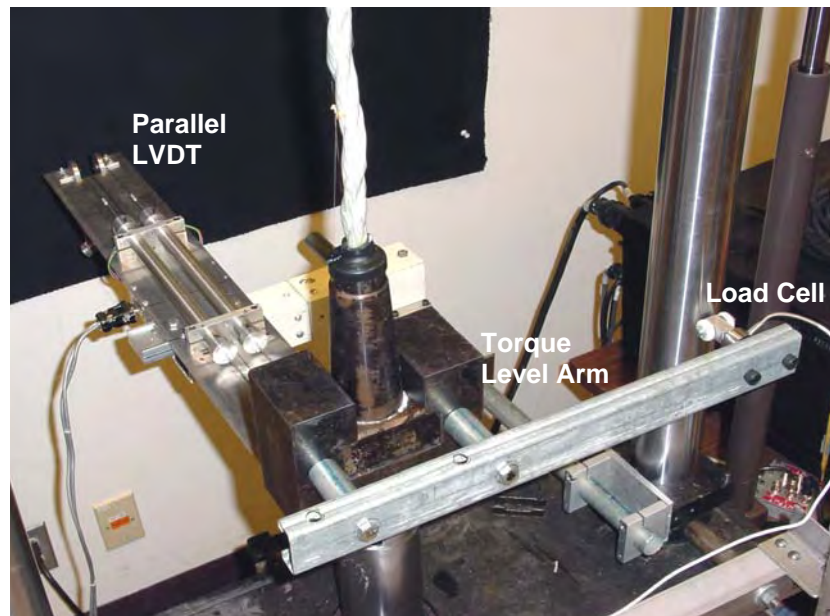


Figure 14 Torque and LVDT measurement devices.

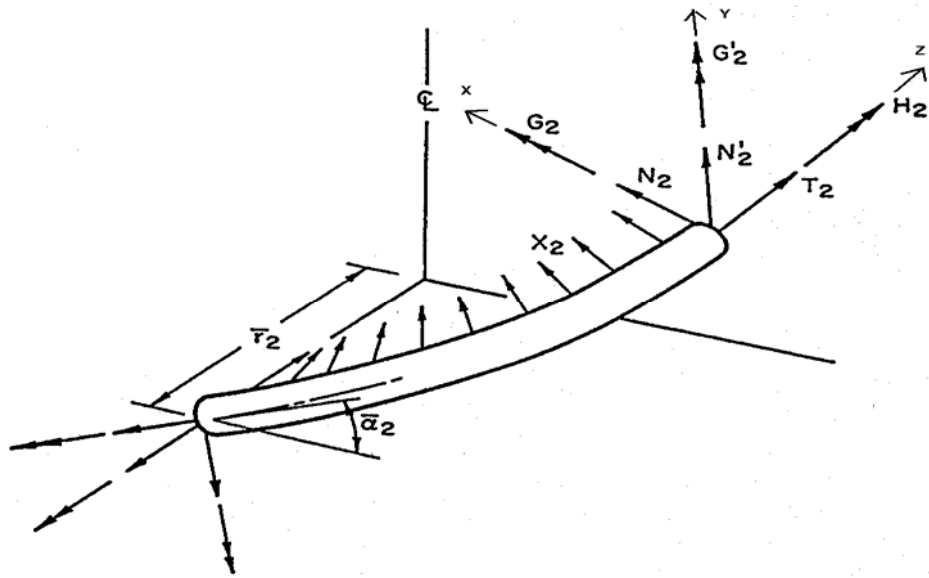


Figure 15 Load, geometry and coordinate system of a fiber strand.

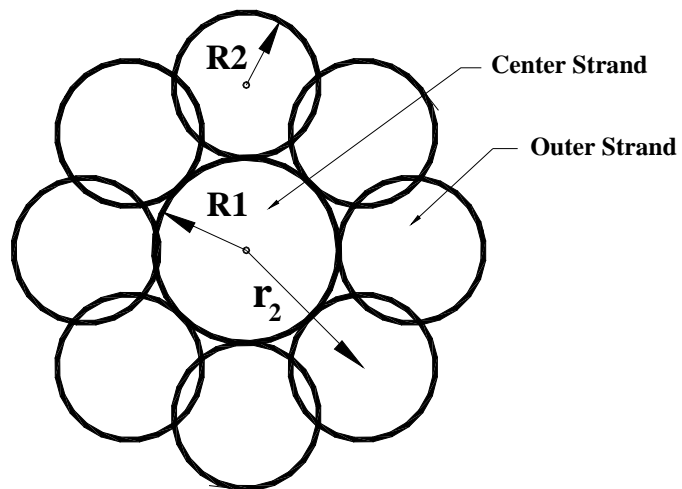
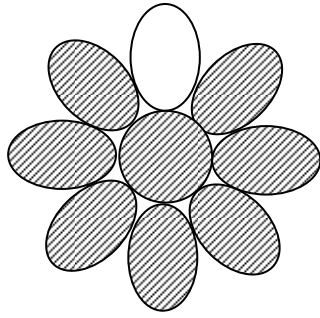
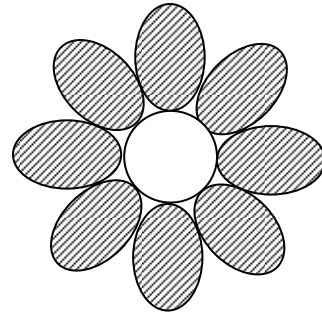


Figure 16 Sectional geometry of a rope element (Mooring rope #1).

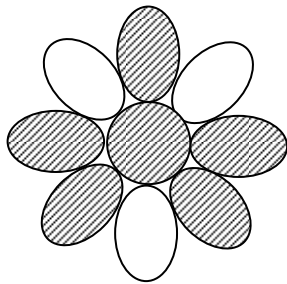


(A)

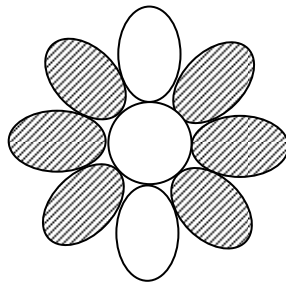


(B)

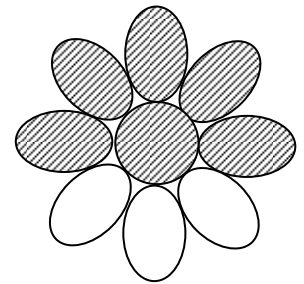
Figure 17 Rope element with one strand cut (Two distinct types of damage).



(C)



(D)



(E)

Figure 18 Rope element with three strands cut (Three distinct types of damage).

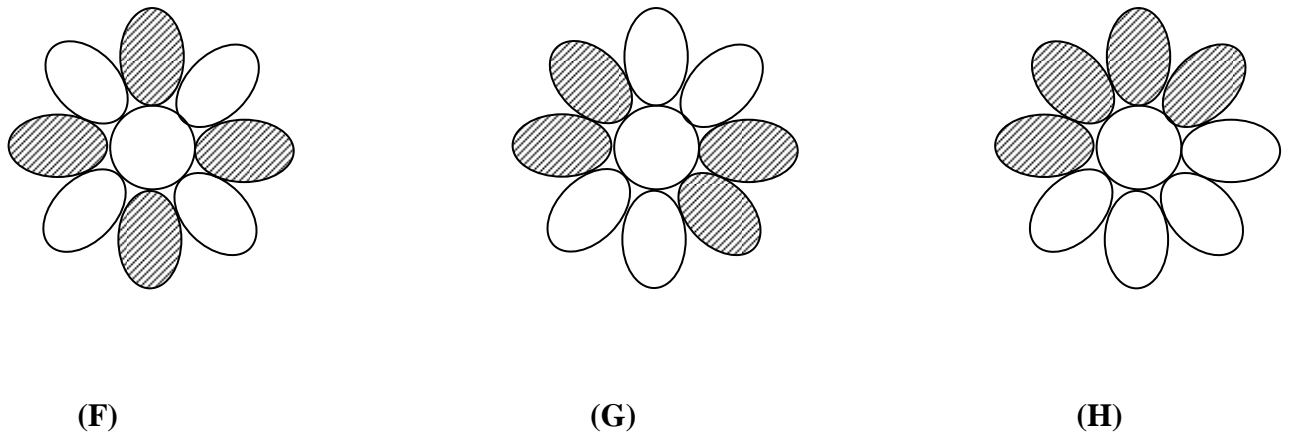


Figure 19 Rope element with five strands cut (Three distinct types of damage).

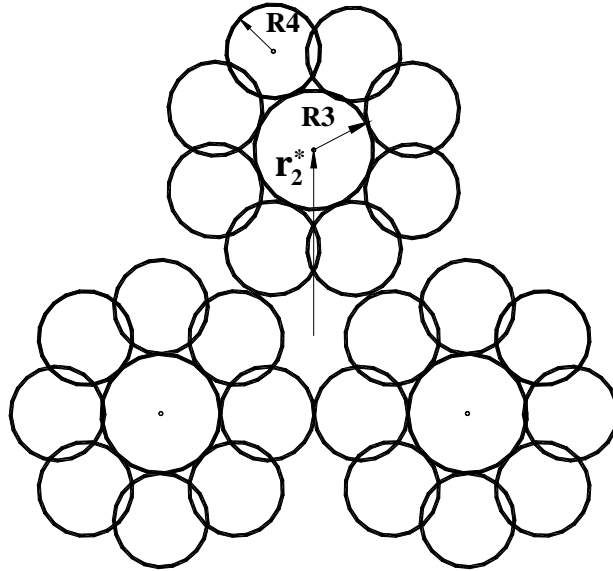


Figure 20 Sectional view of a subrope (Mooring rope #1).

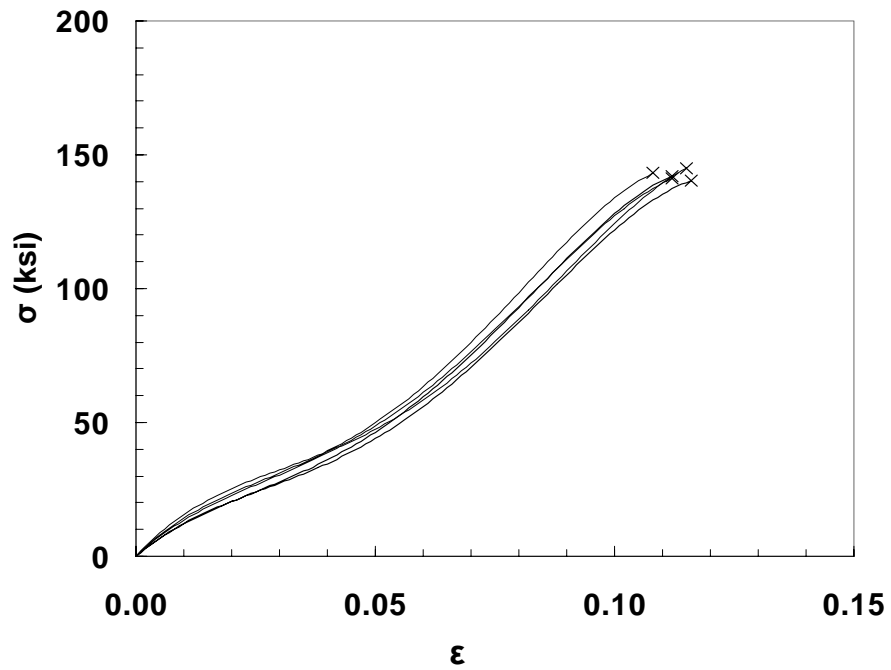


Figure 21 $\sigma - \epsilon$ behavior of polyester yarns (Mooring rope #1).

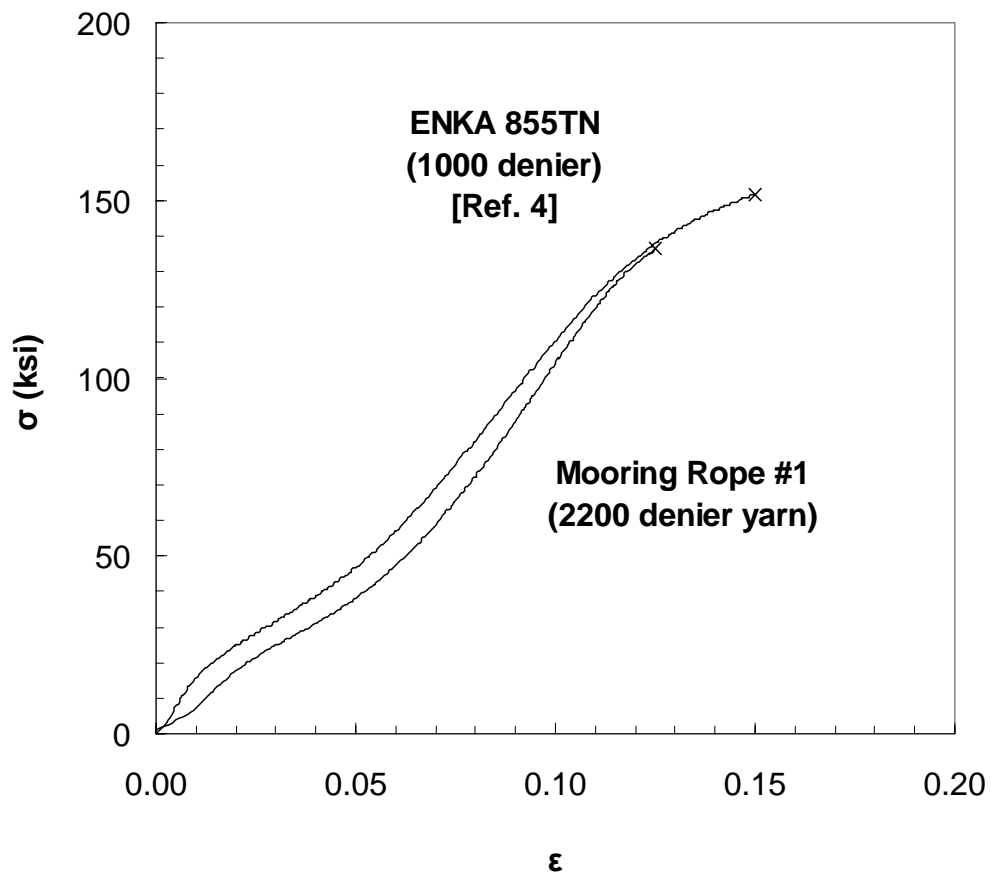


Figure 22 Comparison of test results with published data [4] (polyester yarns).

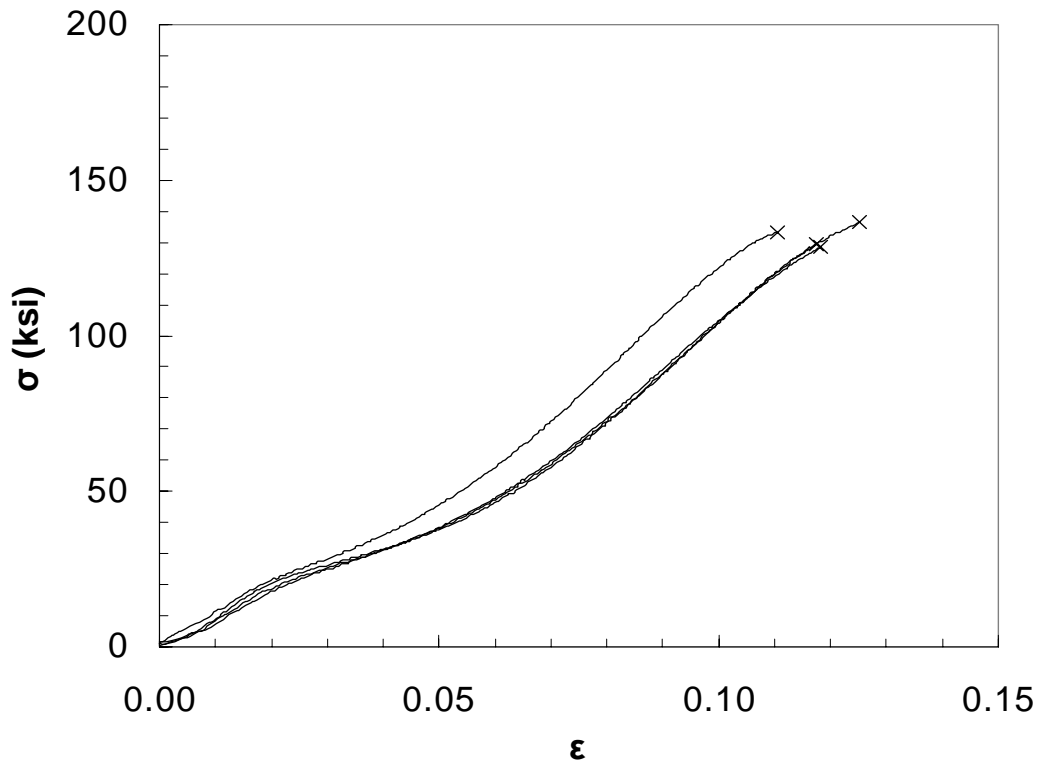


Figure 23 $\sigma - \varepsilon$ behavior of polyester-rope strands (Mooring rope #1).



Figure 24 Failure mode of polyester-rope strands (Mooring rope #1).

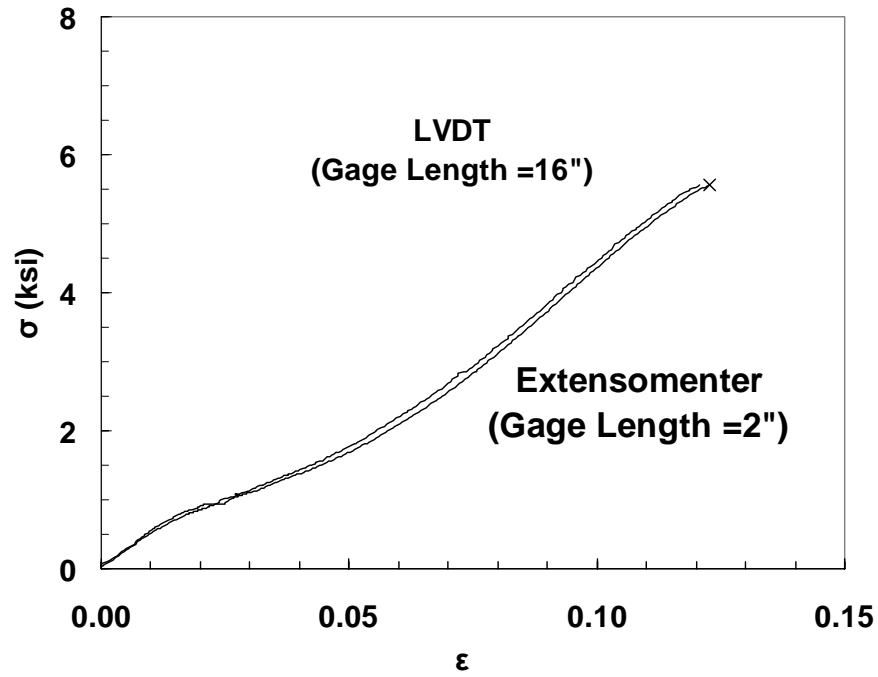


Figure 25 Comparison of measured strains (in rope element) by a LVDT and an extensometer.

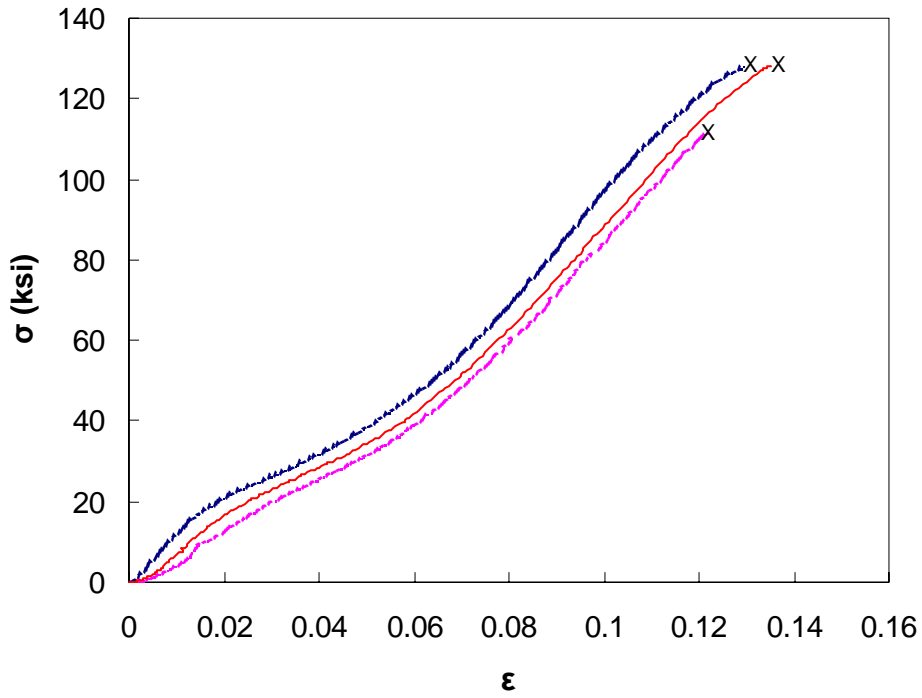


Figure 26 $\sigma - \epsilon$ behavior of undamaged rope elements (Mooring rope #1).

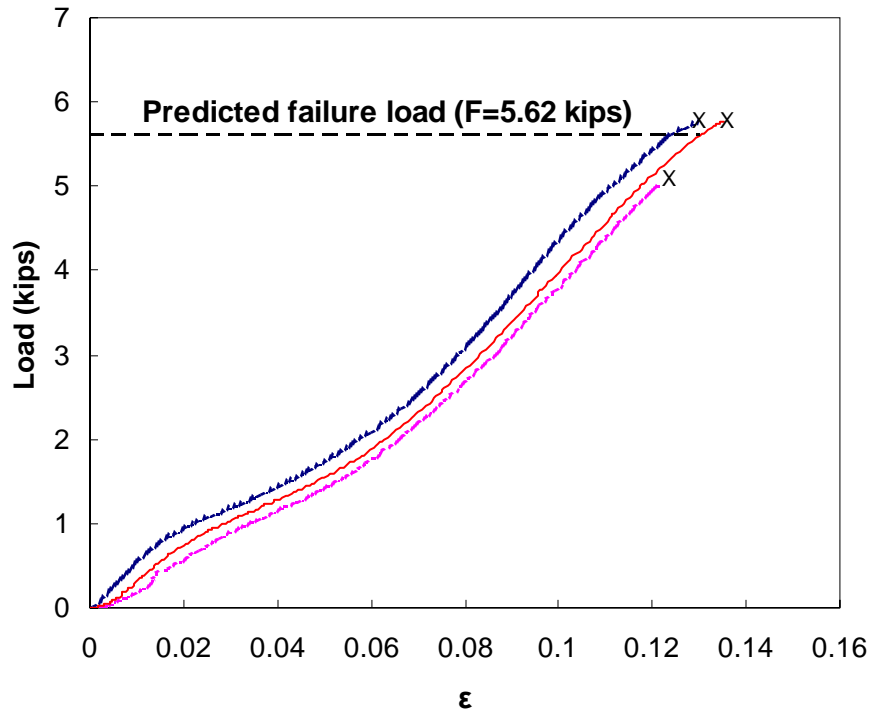


Figure 27 $P - \epsilon$ response of undamaged rope elements (Mooring rope #1).

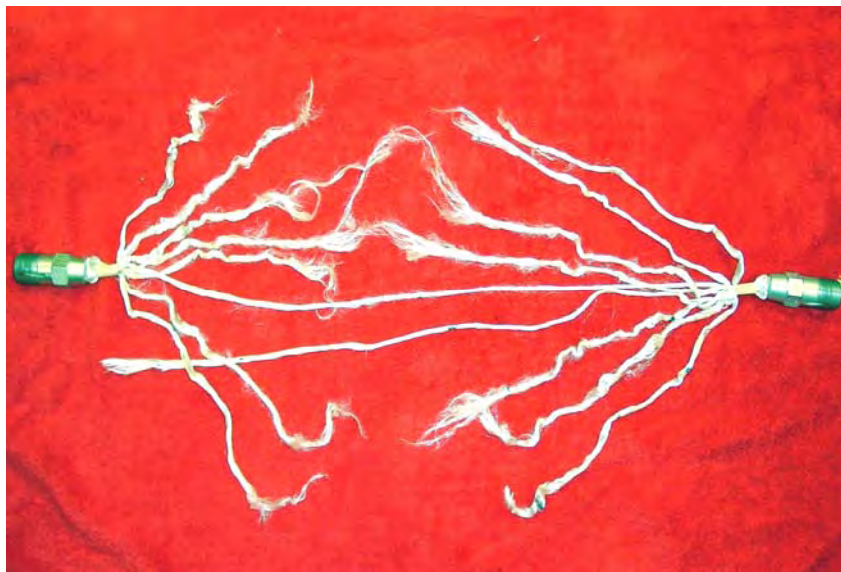


Figure 28 Rope element failure mode (Mooring rope #1).

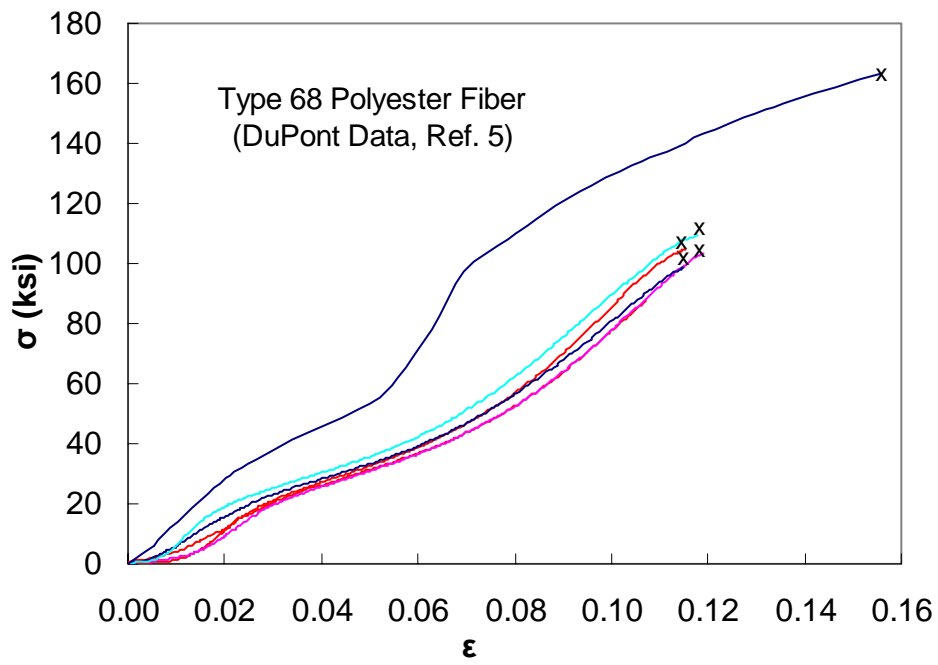


Figure 29 $\sigma - \varepsilon$ behavior of undamaged rope elements (Mooring rope #2).

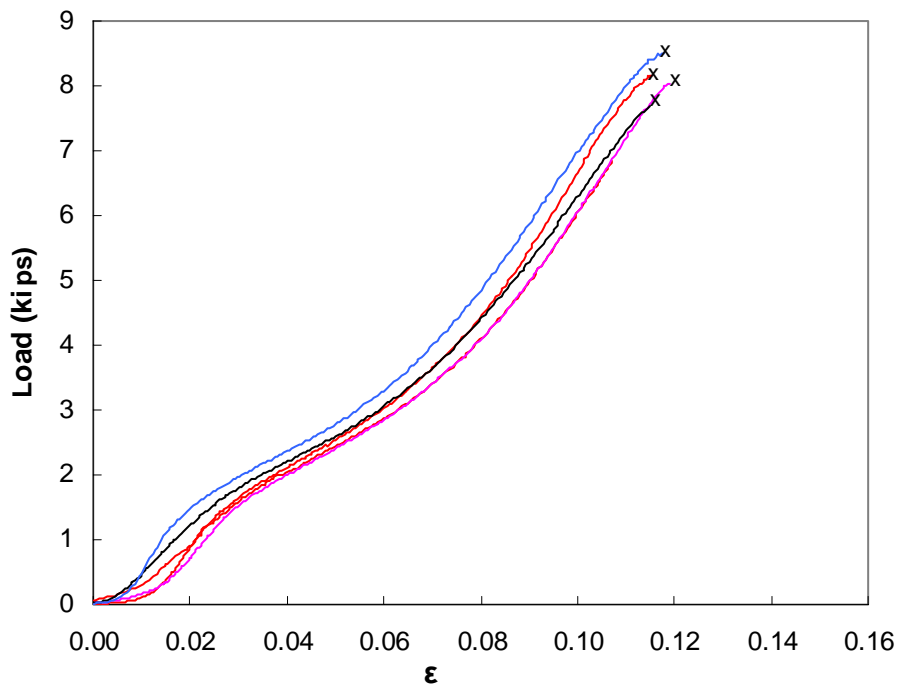


Figure 30 $P - \varepsilon$ response of undamaged rope elements (Mooring rope #2).

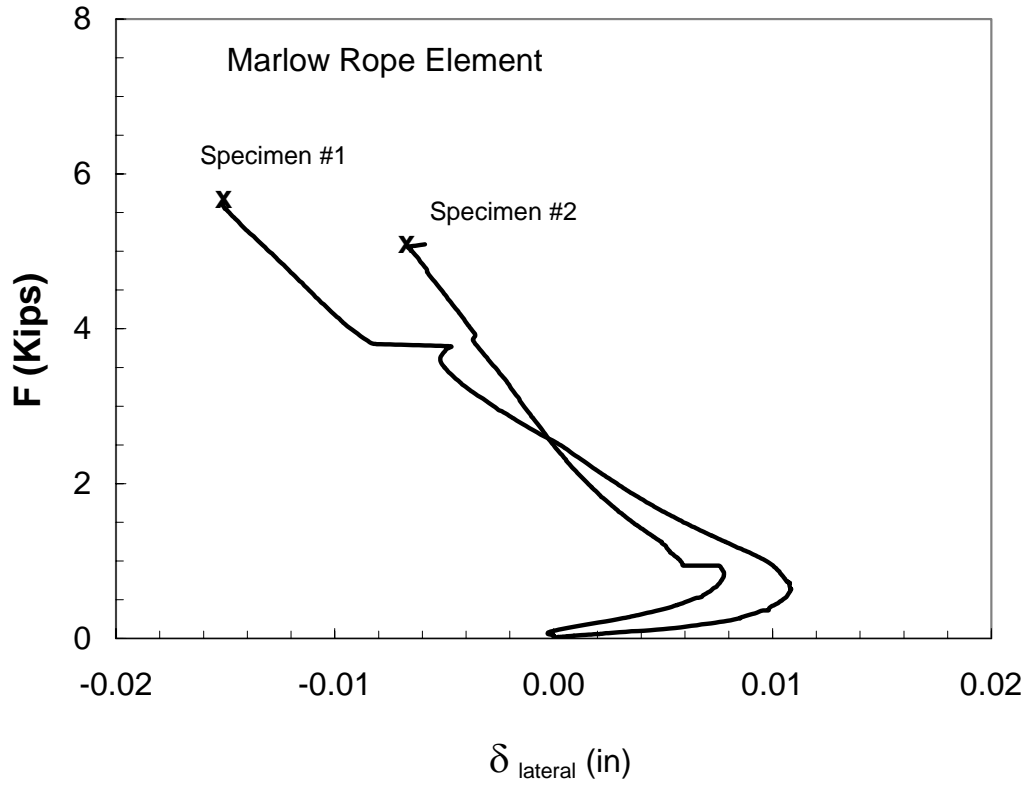


Figure 31 Element diameter change during rope element test (undamaged element).

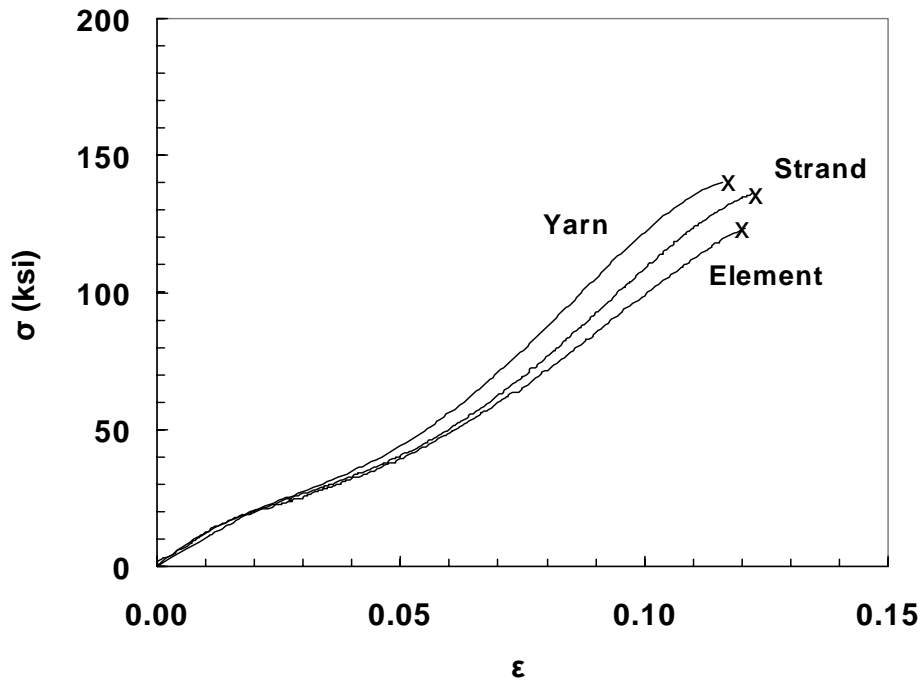


Figure 32 Comparison of stress-strain relationships among yarn, strand, and element (Mooring rope #1).

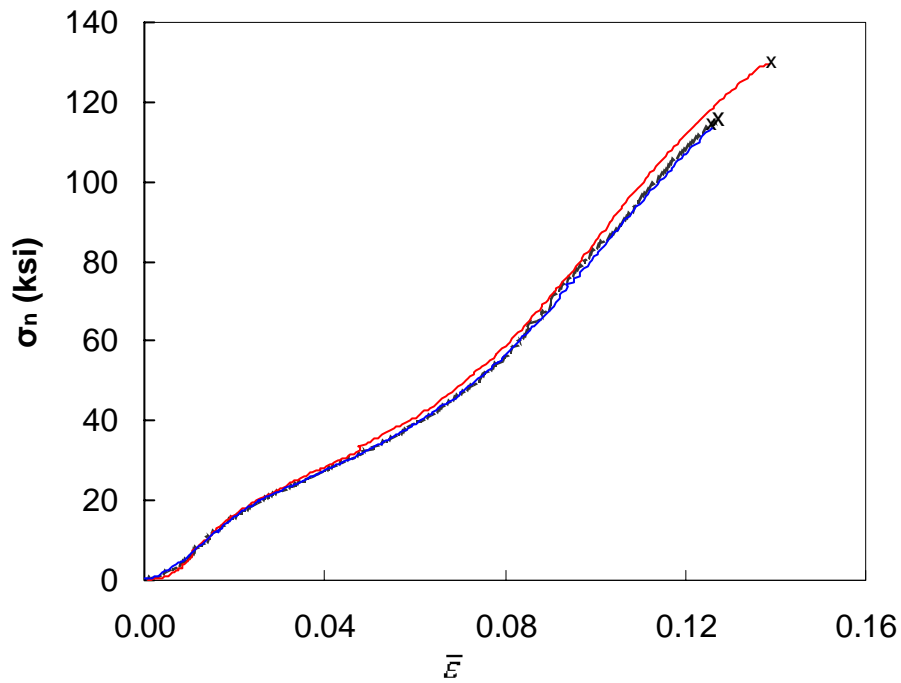


Figure 33 $\sigma_n - \bar{\epsilon}$ behavior of rope elements with 1 strand cut (Mooring rope #1).

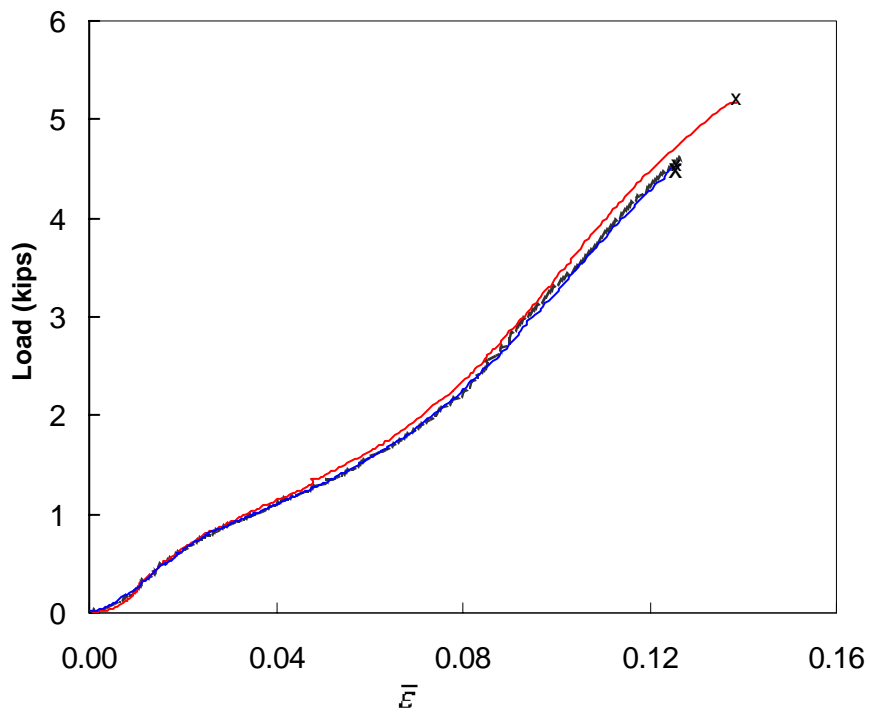


Figure 34 $P - \bar{\epsilon}$ behavior of rope elements with 1 strand cut (Mooring rope #1).

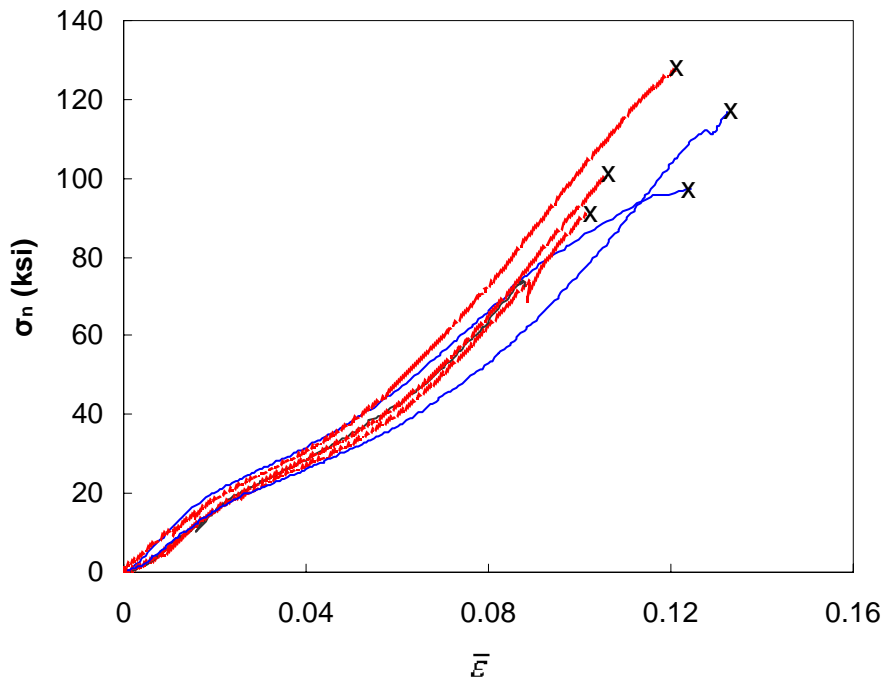


Figure 35 $\sigma_n - \bar{\epsilon}$ behavior of rope elements with 3 strands cut (Mooring rope #1).

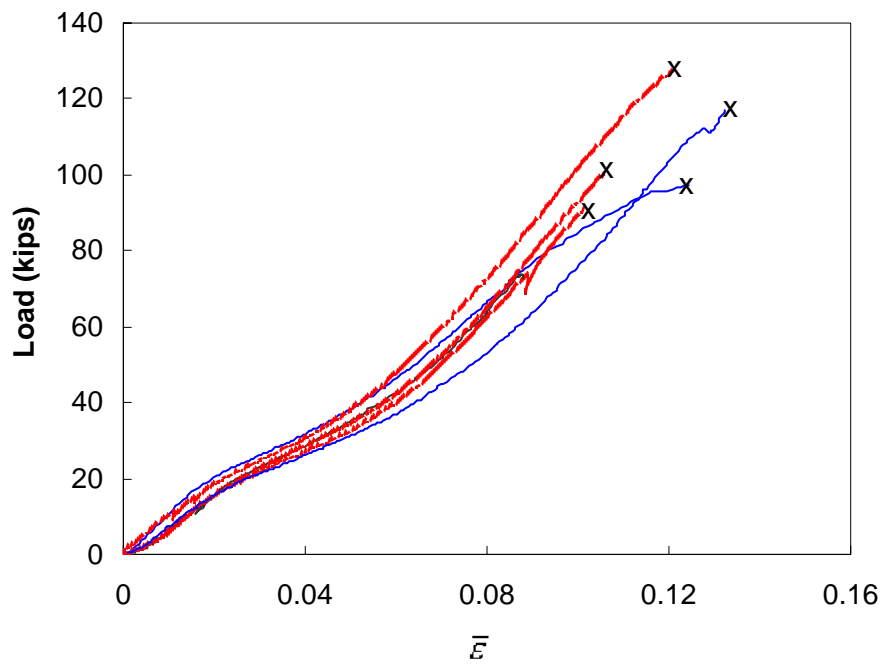


Figure 36 $P - \bar{\epsilon}$ behavior of rope elements with 3 strands cut (Mooring rope #1).

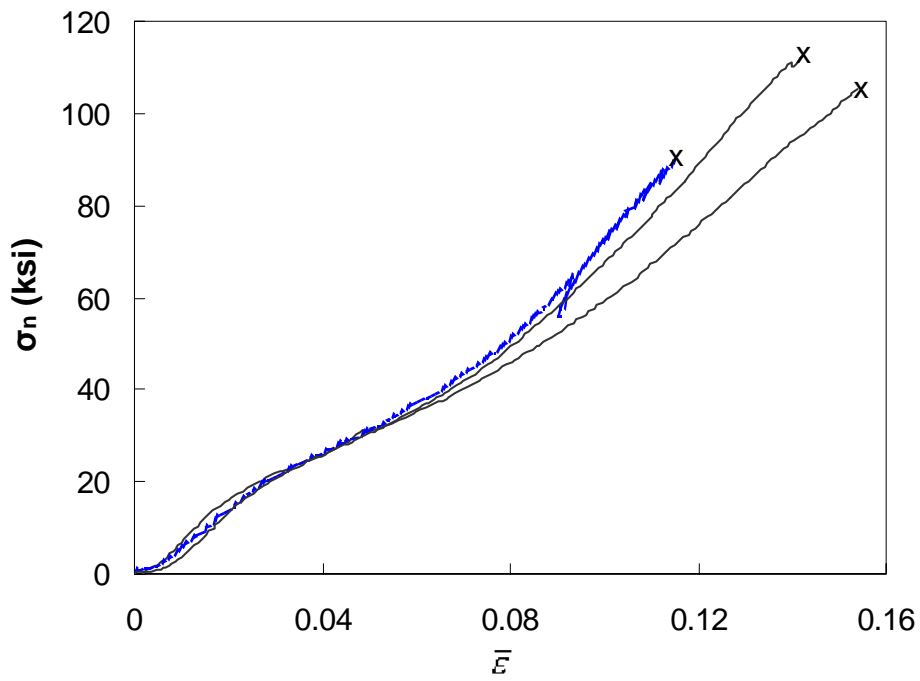


Figure 37 $\sigma_n - \bar{\epsilon}$ behavior of rope elements with 5 strands cut (Mooring rope #1).

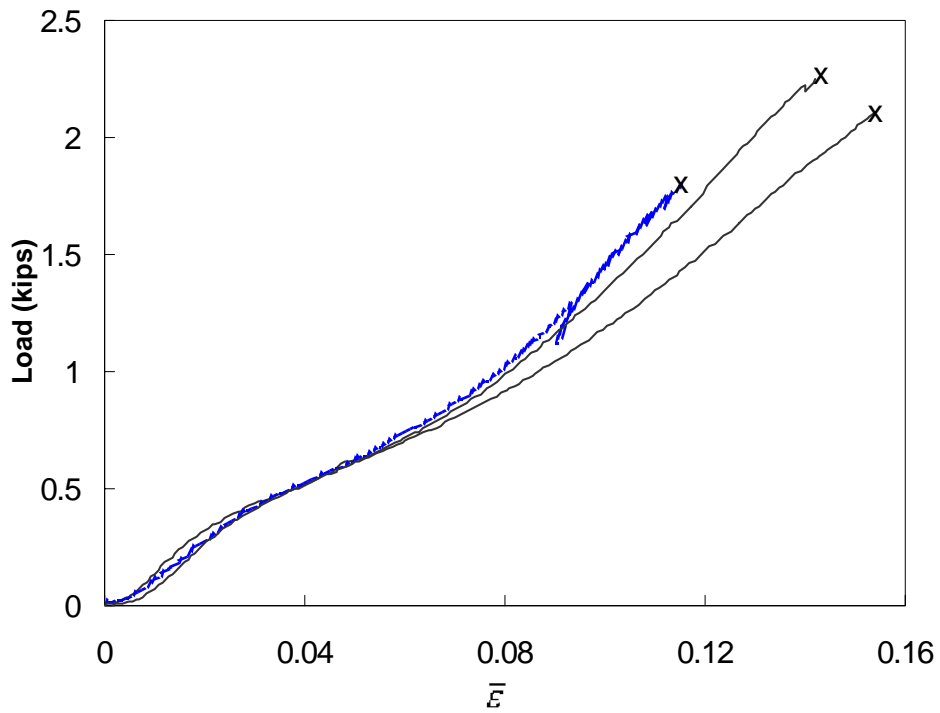


Figure 38 $P - \bar{\epsilon}$ behavior of rope elements with 5 strands cut (Mooring rope #1).

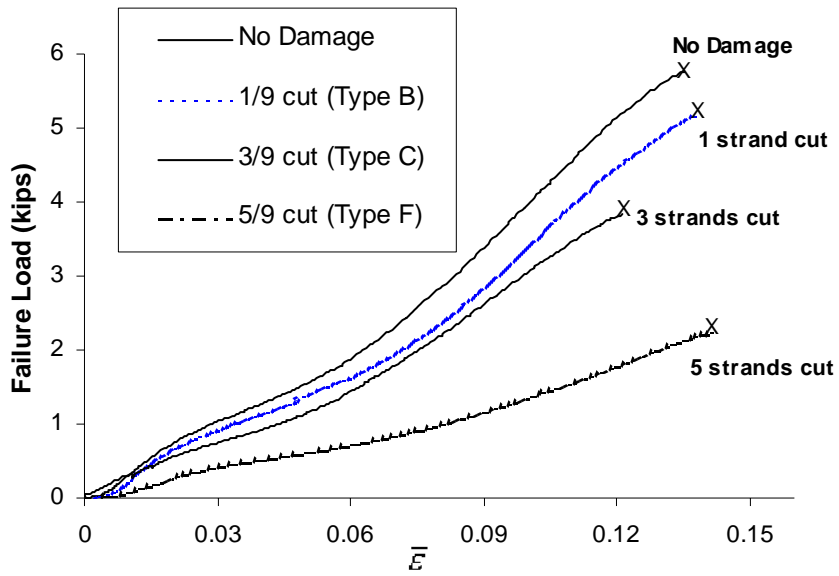


Figure 39 $P - \bar{\epsilon}$ responses of rope elements with damage (Mooring rope #1)

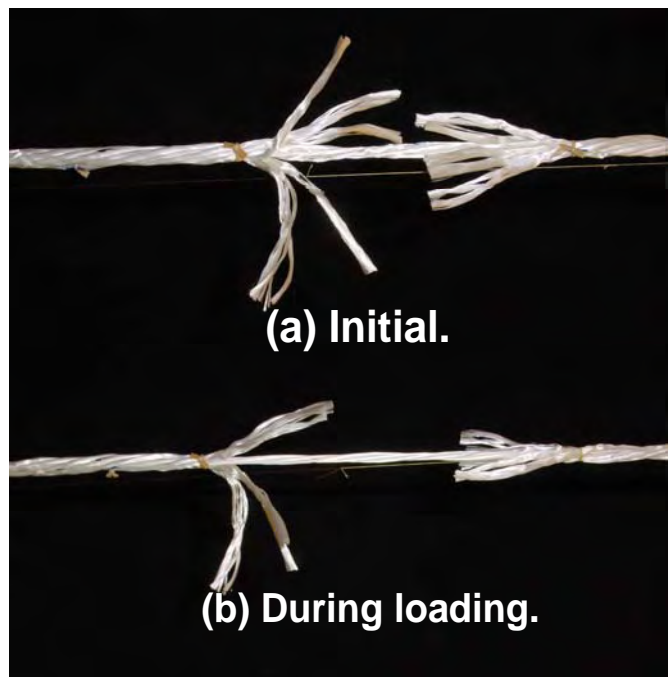


Figure 40 Cut strand migration during rope element test.

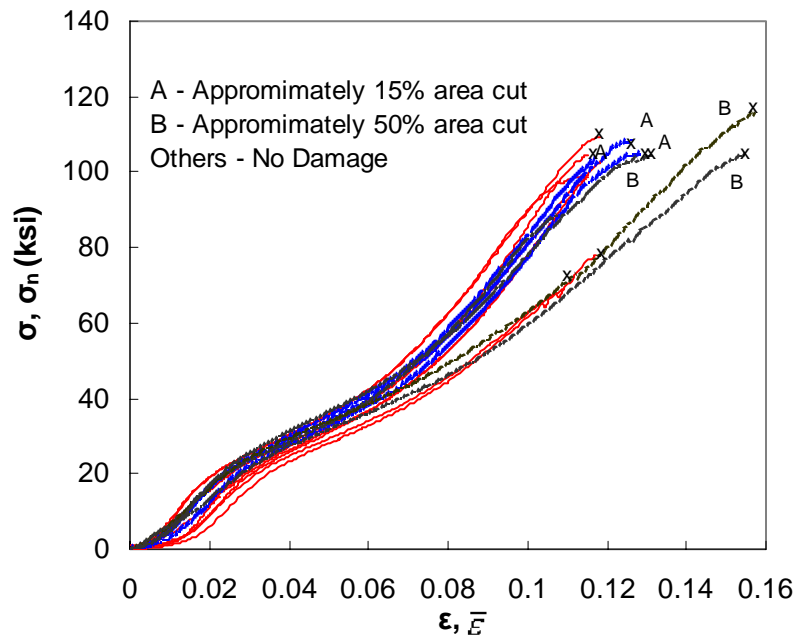


Figure 41 $\sigma_n - \bar{\varepsilon}$ and $\sigma - \varepsilon$ behavior of Mooring rope #2 elements (undamaged and damaged).

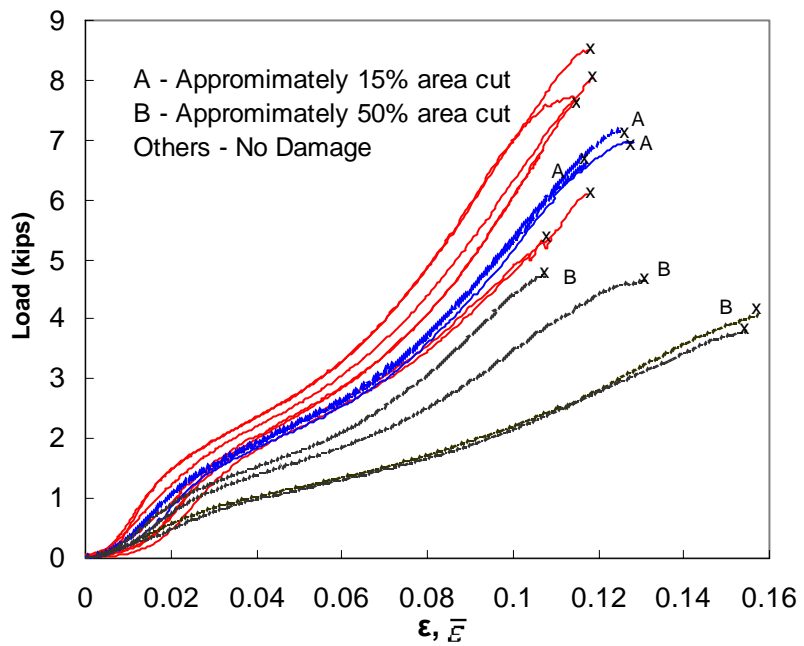


Figure 42 $P - \bar{\varepsilon}$ responses of Mooring rope #2 elements (undamaged and damaged).



Figure 43 Rope elements showing cut and failed fibers (Mooring rope #2).

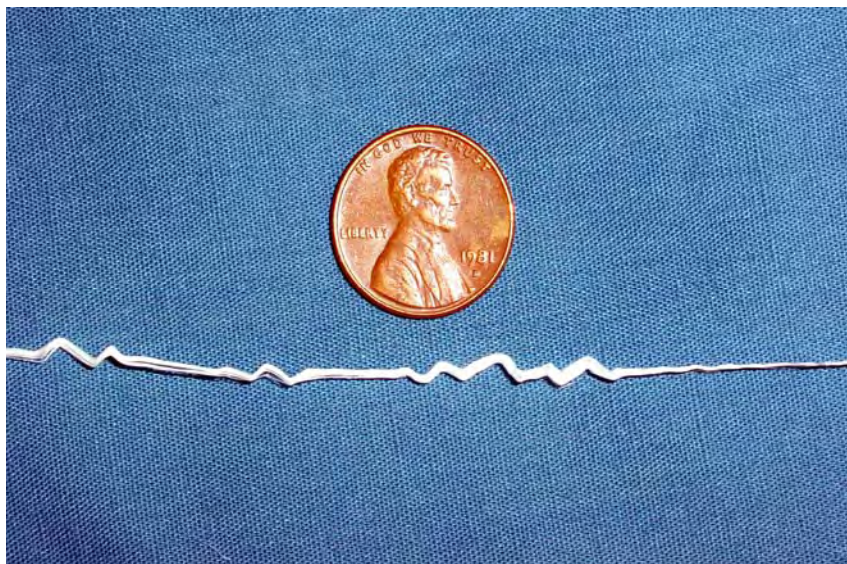


Figure 44 Polyester yarn kinking.

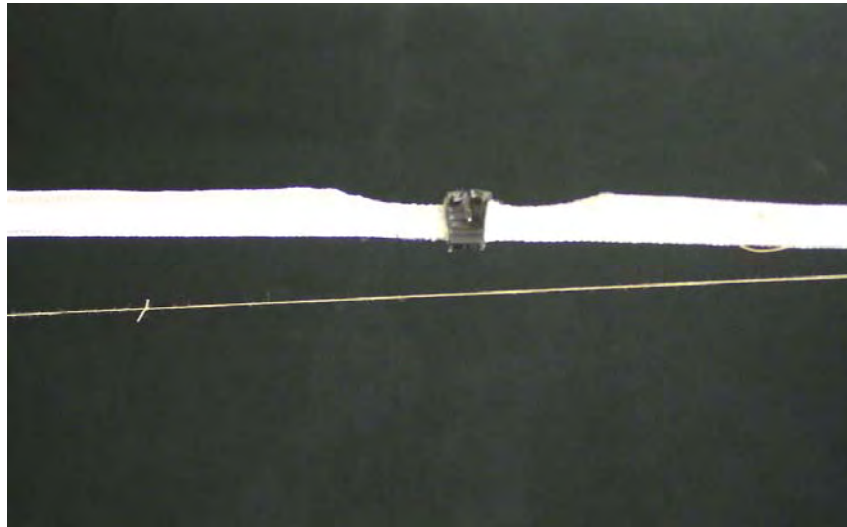


Figure 45 Neck-down of cut fiber-strand migration during rope element test (Mooring rope #2).

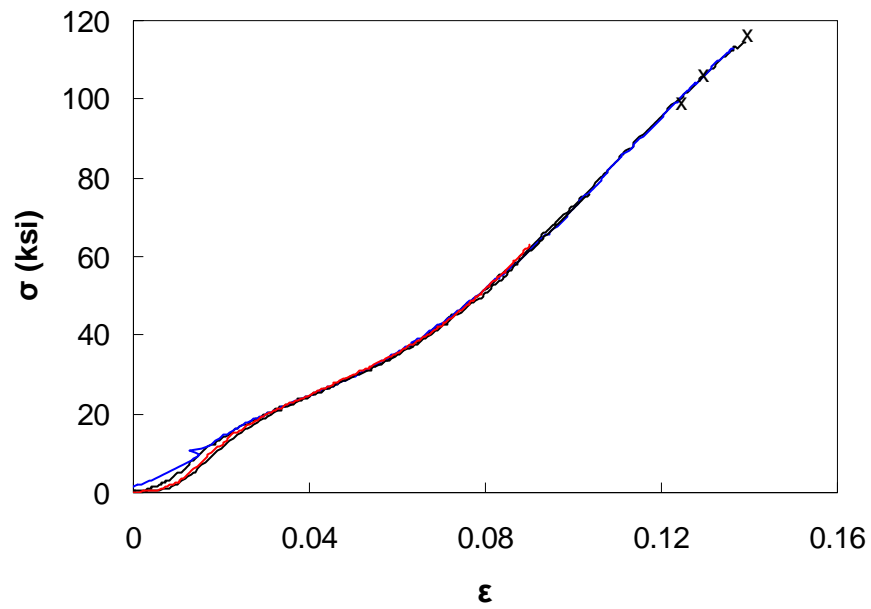


Figure 46 $\sigma - \epsilon$ behavior of undamaged subropes (Mooring rope #1).

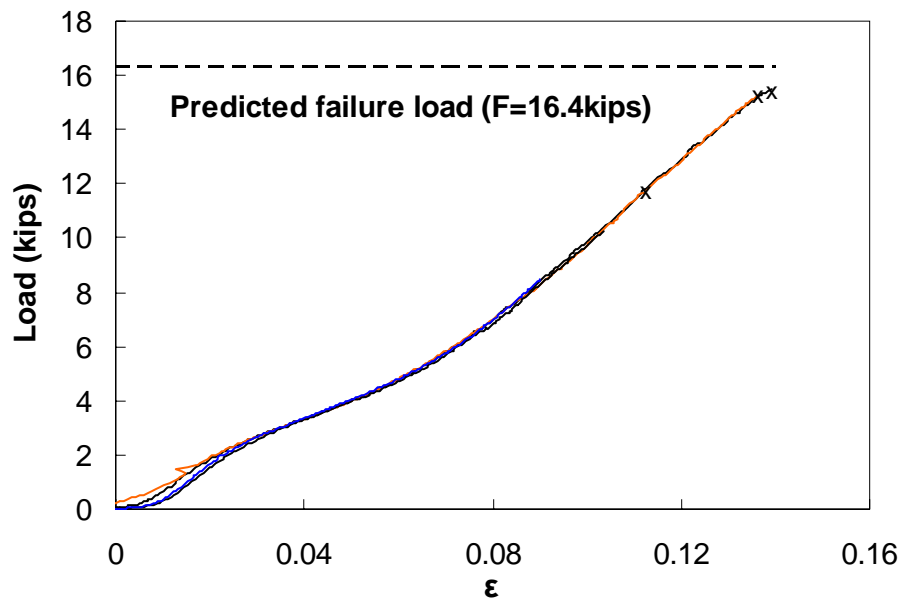


Figure 47 $P - \epsilon$ response of undamaged subropes (Mooring rope #1).

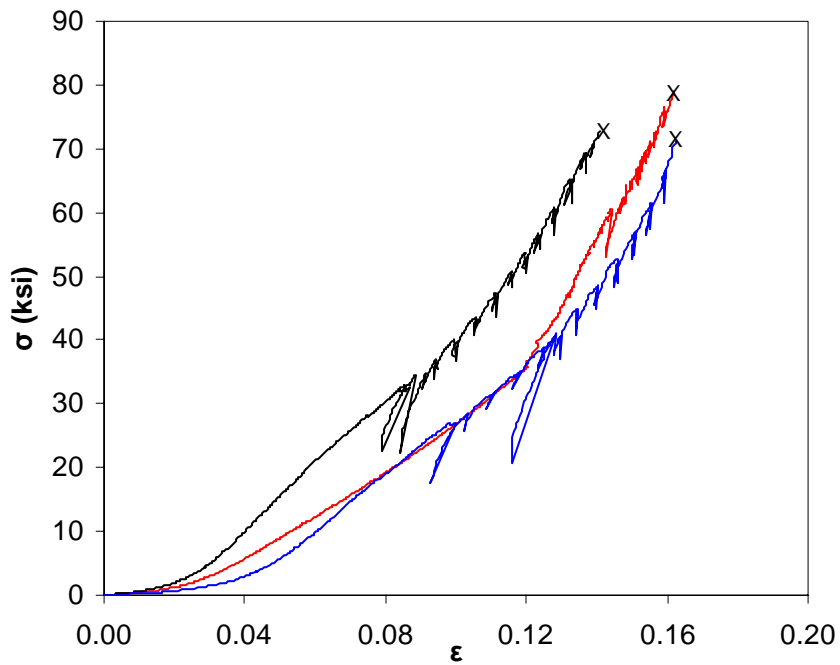


Figure 48 $\sigma - \epsilon$ behavior of undamaged subropes (Mooring rope #2).

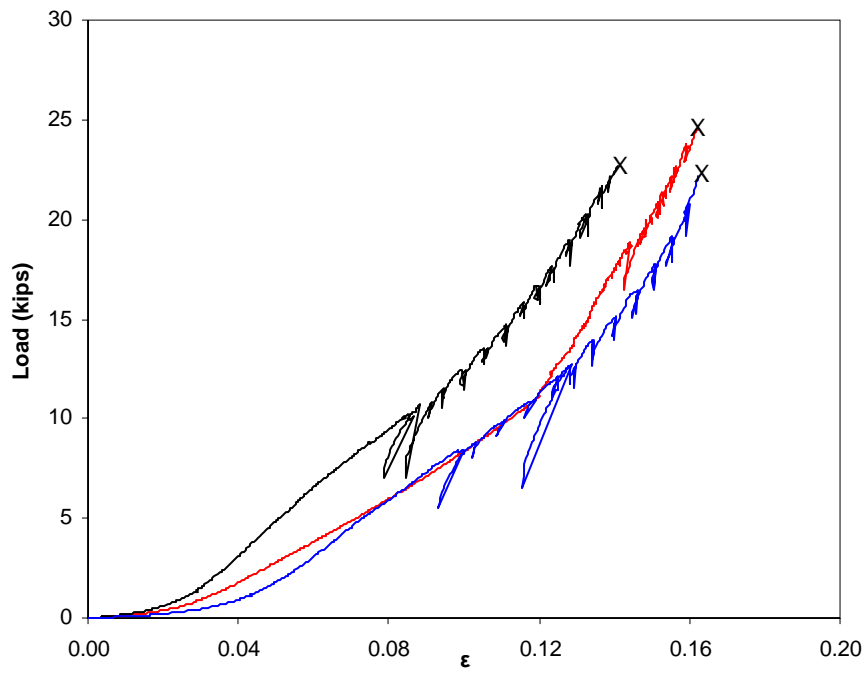


Figure 49 $P - \varepsilon$ response of undamaged subropes (Mooring rope #2).

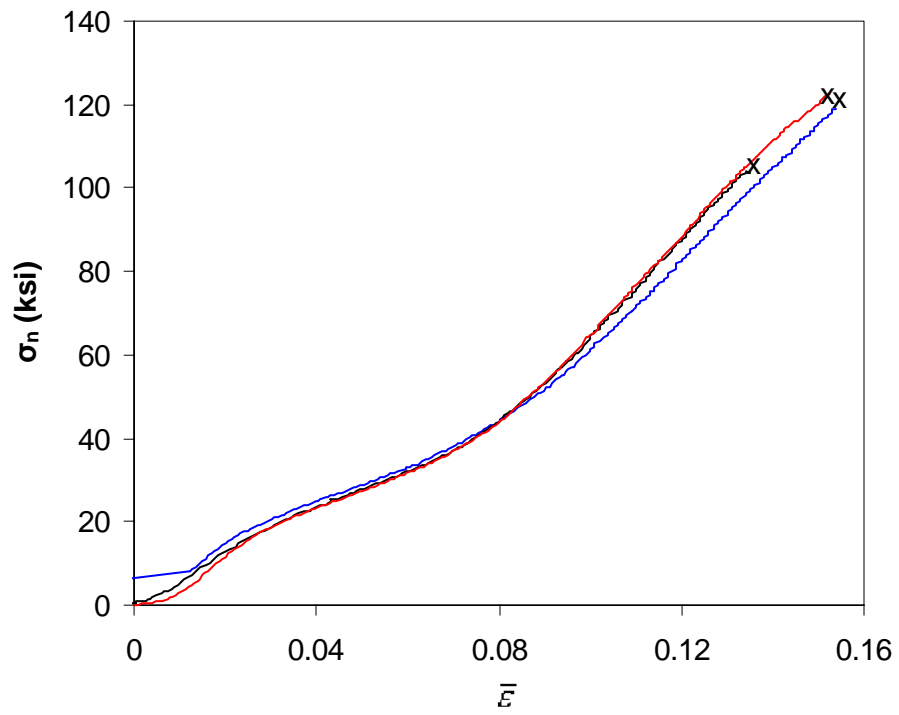


Figure 50 $\sigma_n - \bar{\varepsilon}$ behavior of subropes with 5 strands cut (Mooring rope #1).

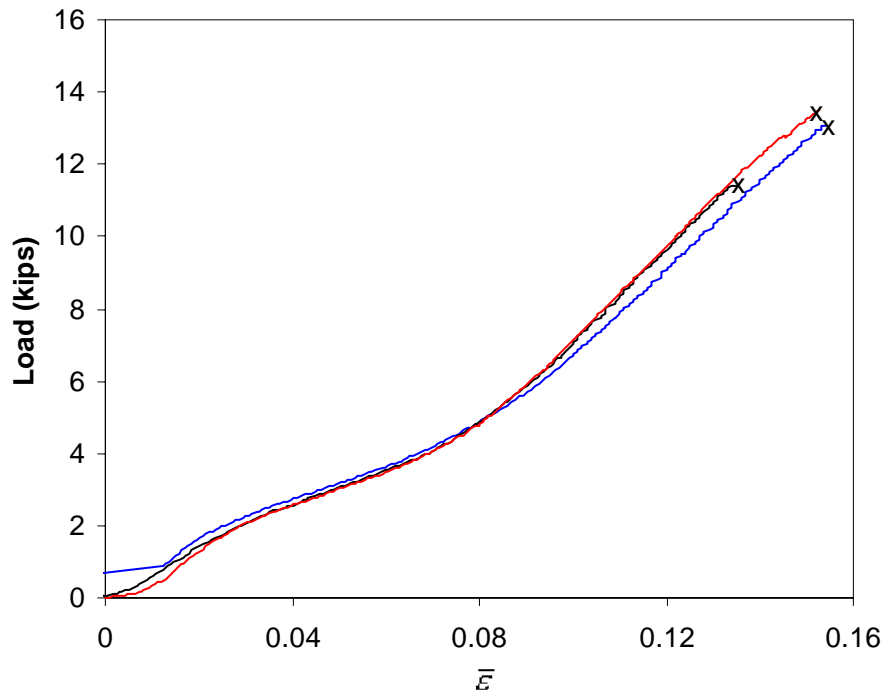


Figure 51 $P - \bar{\epsilon}$ response of subropes with 5 strands cut (Mooring rope #1).

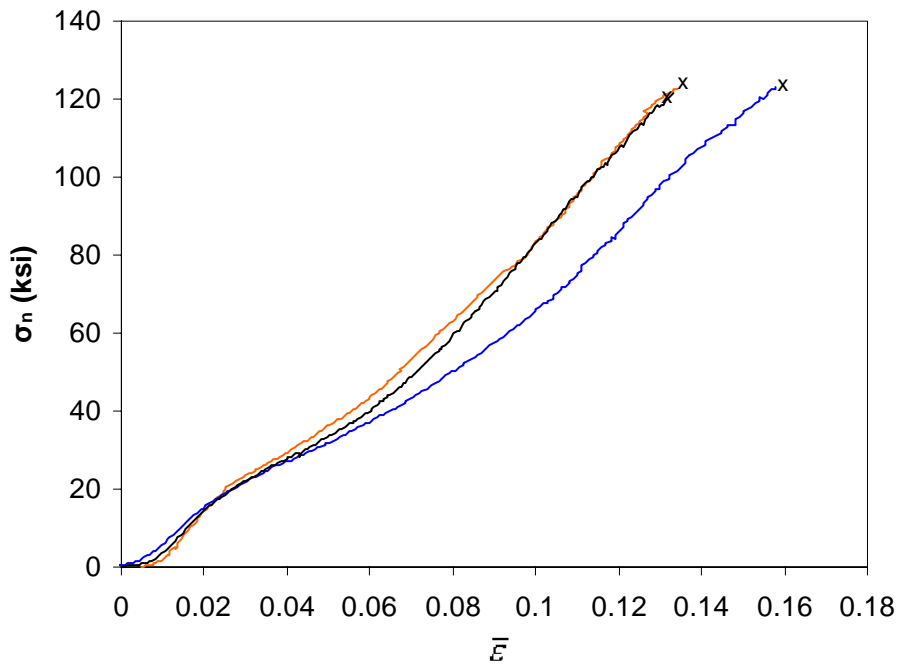


Figure 52 $\sigma_n - \bar{\epsilon}$ behavior of subropes with 9 strands cut (Mooring rope #1).
(5 strands cut in one element, and 4 strands in second element)

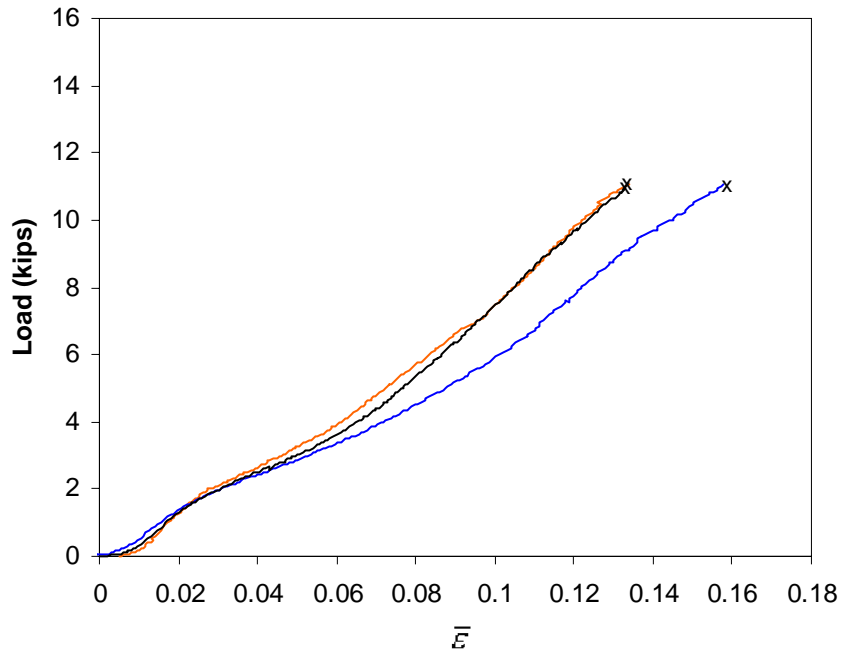


Figure 53 $P - \bar{\epsilon}$ response of subropes with 9 strands cut (Mooring rope #1).
(5 strands cut in one element, and 4 strands in second element)

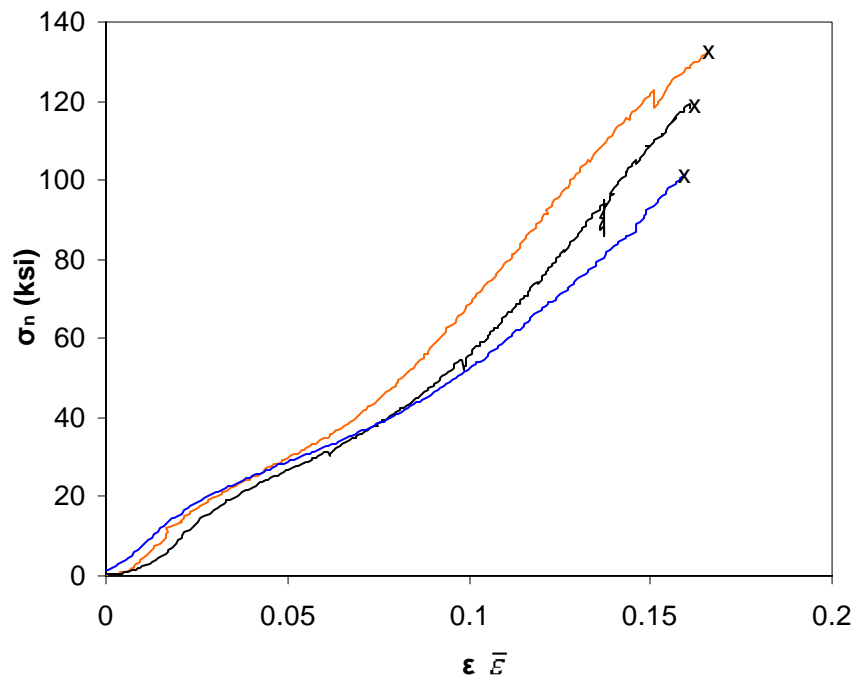


Figure 54 $\sigma_n - \bar{\epsilon}$ behavior of subropes with 13 strands cut (Mooring rope #1).
(9 strands cut in one element, and 2 strands in each of other two elements)

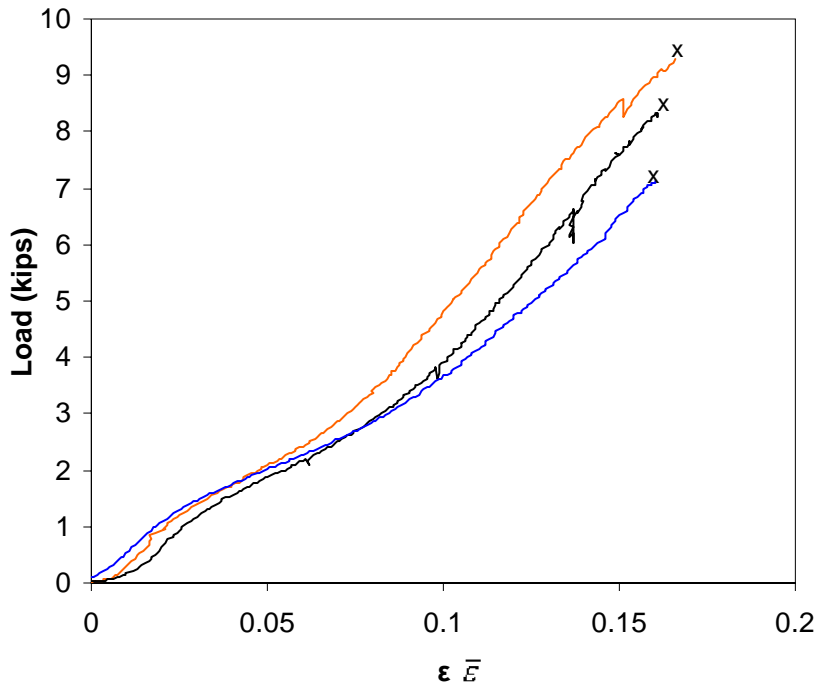


Figure 55 $P - \bar{\epsilon}$ response of subropes with 13 strands cut (Mooring rope #1).
 (9 strands cut in one element, and 2 strands in each of other two elements)



Figure 56 Damaged subrope failure mode (Mooring rope #1).
 (5 strands cut in one element, and 4 in another element)



Figure 57 Local melting of polyester fibers during break of damaged subrope (Mooring subrope #1).

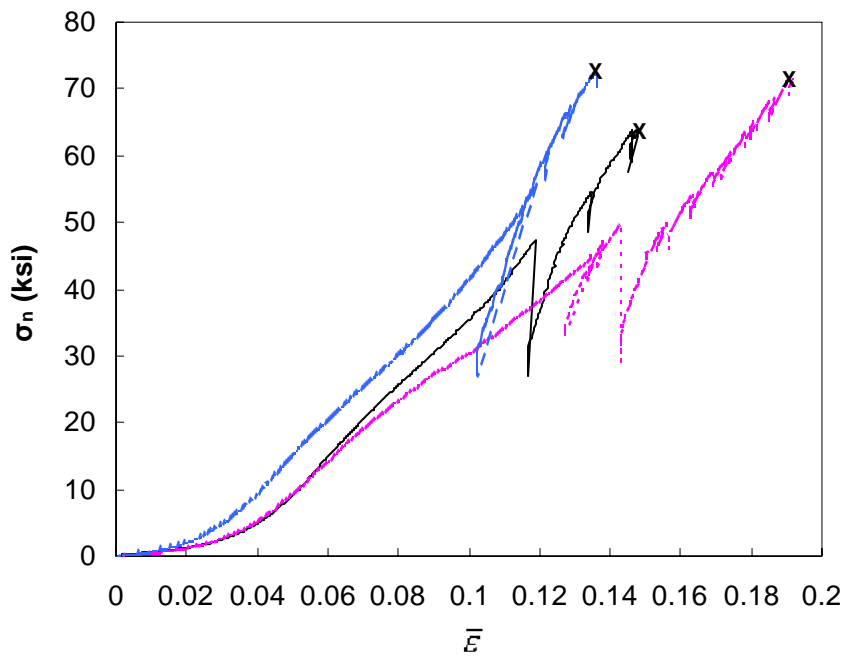


Figure 58 $\sigma_n - \bar{\epsilon}$ behavior of subropes with 1 element cut (Mooring rope #2).

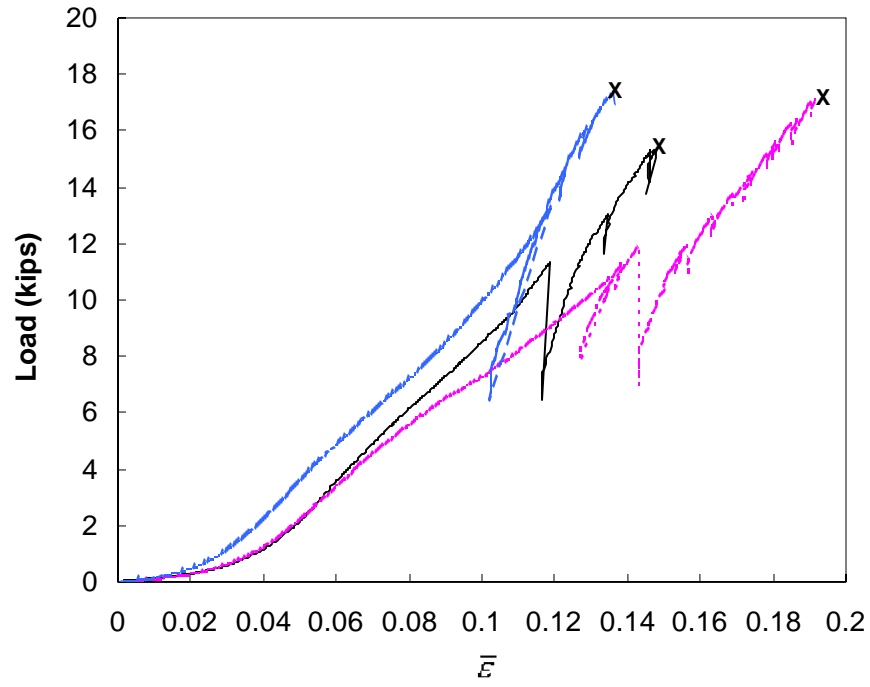


Figure 59 $P - \bar{\epsilon}$ response of subropes with 1 element cut (Mooring rope #2).

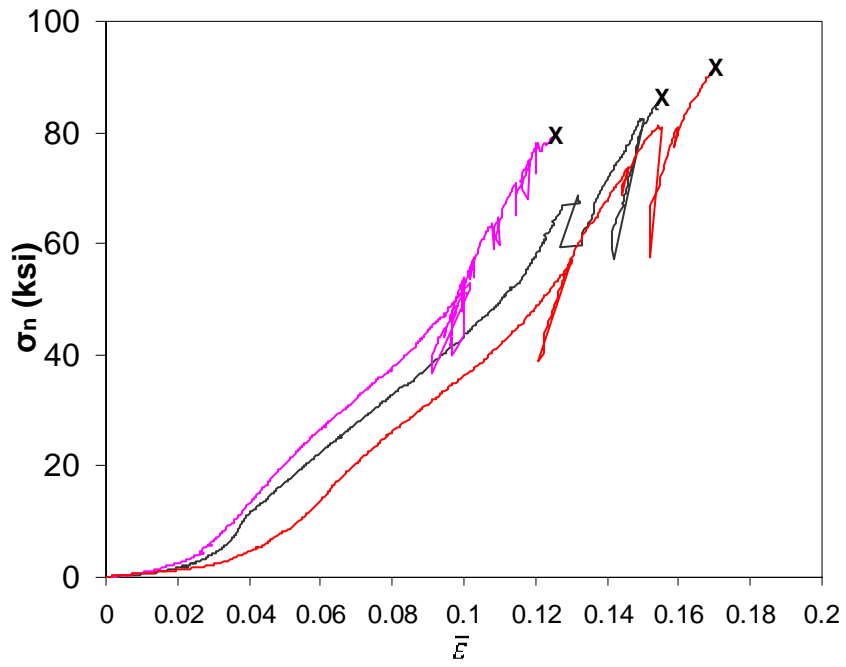


Figure 60 $\sigma_n - \bar{\epsilon}$ behavior of subropes with 2 elements cut (Mooring rope #2).

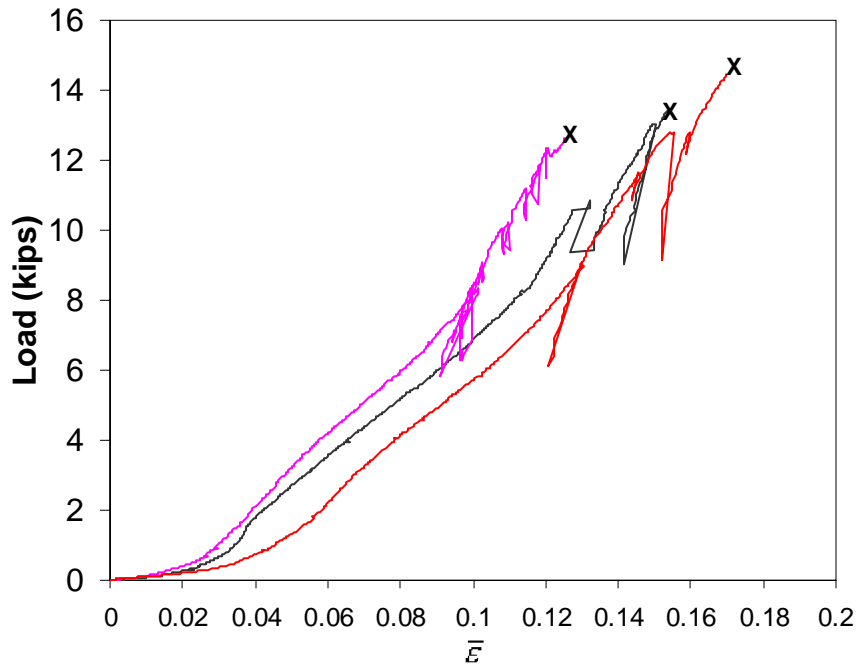


Figure 61 $P - \bar{\epsilon}$ response of subropes with 2 elements cut (Mooring rope #2).

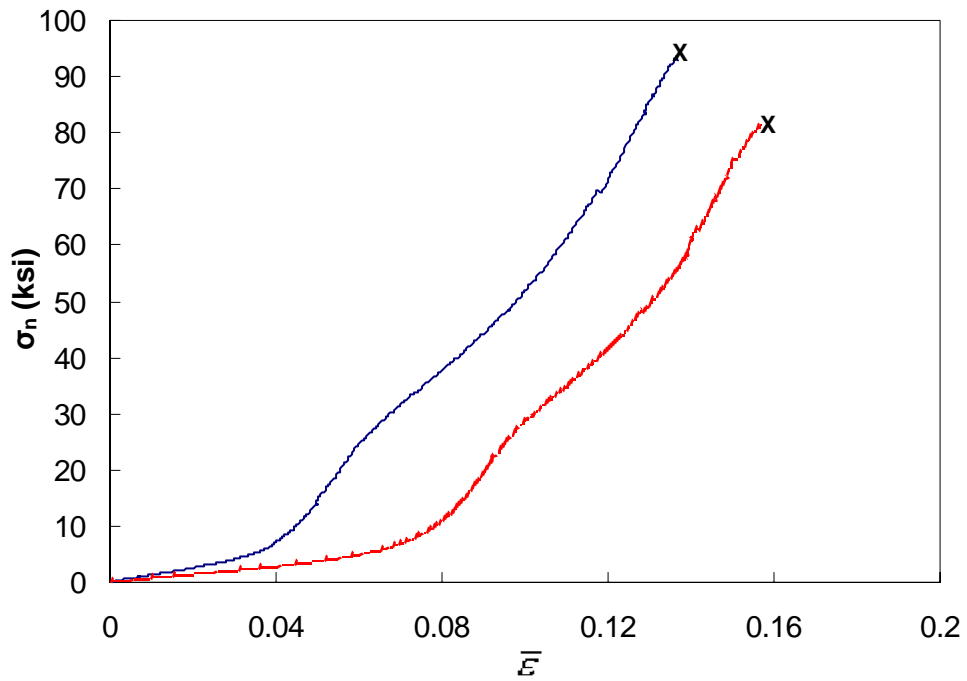


Figure 62 $\sigma_n - \bar{\epsilon}$ behavior of subropes with 3 elements cut (Mooring rope #2).

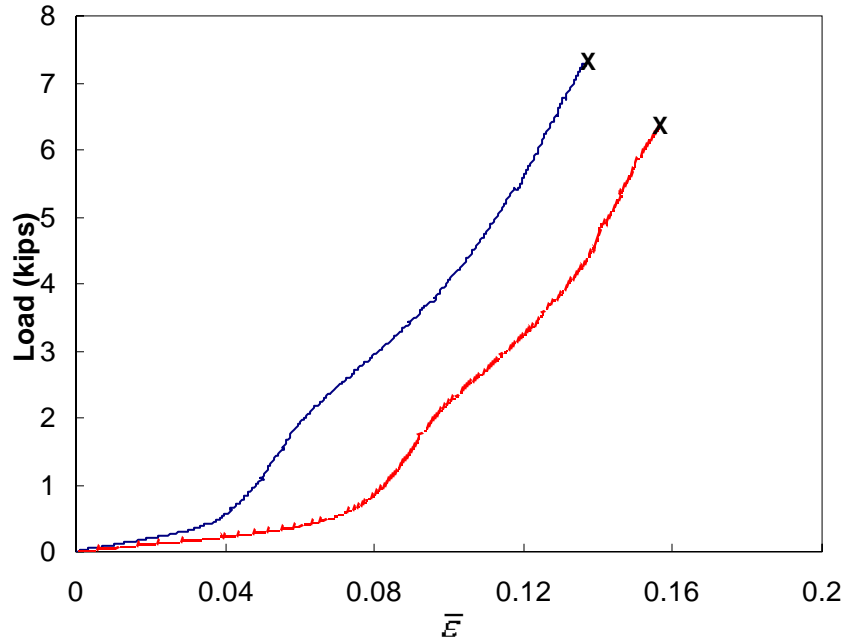


Figure 63 $P - \bar{\epsilon}$ response of subropes with 3 elements cut (Mooring rope #2).

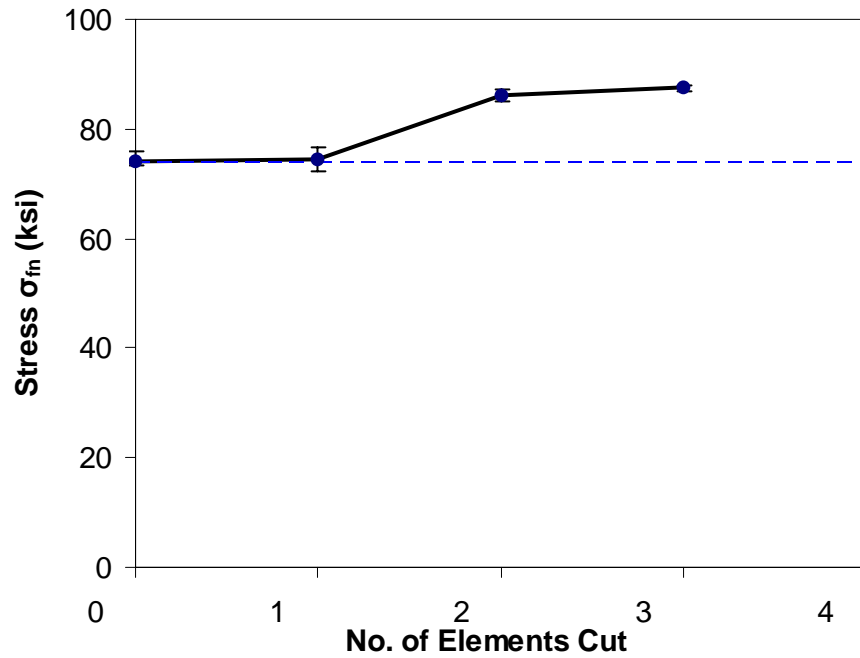


Figure 64 Subrope failure stress (Mooring rope #2) with different rope elements cut.

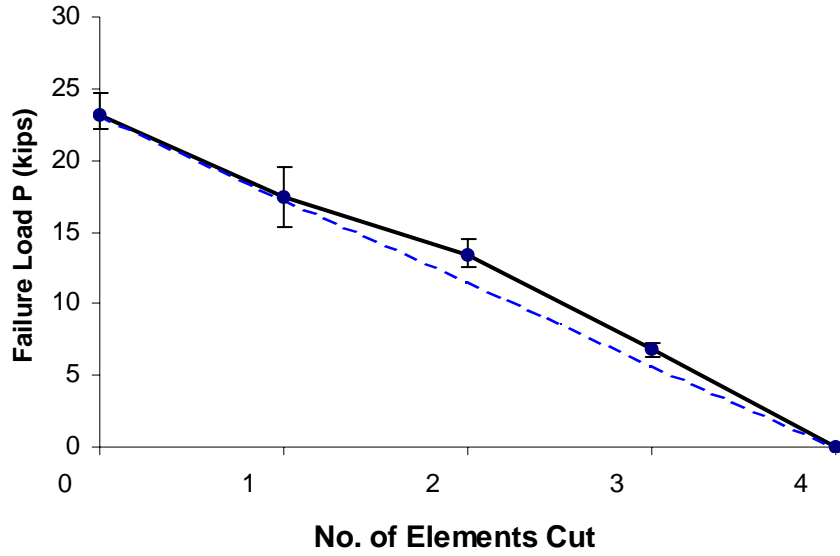


Figure 65 Failure strength of subropes with different elements cut (Mooring rope #2).

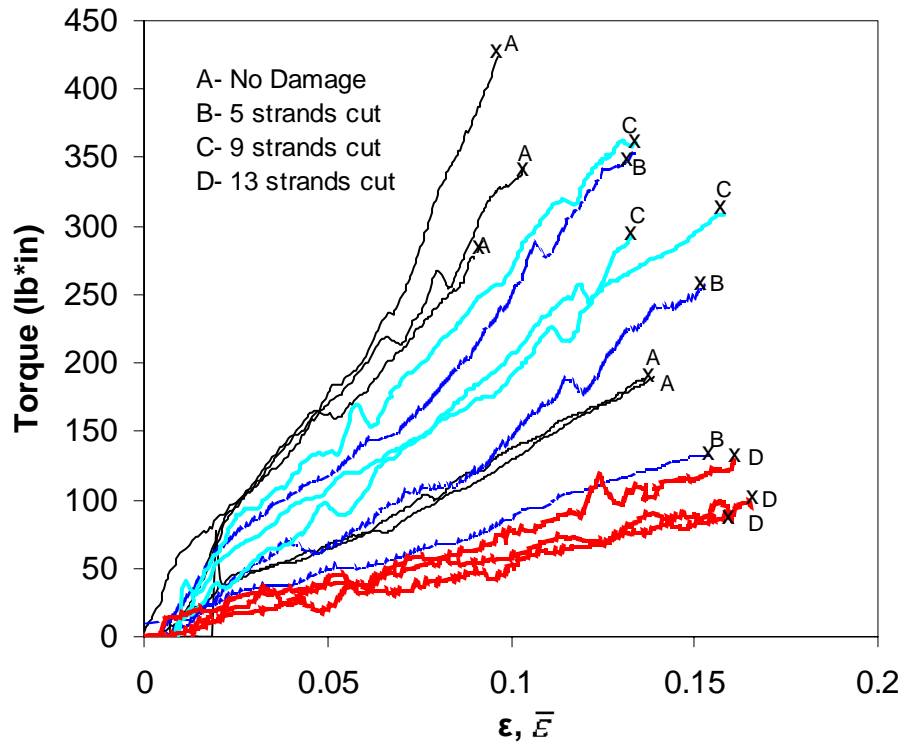


Figure 66 Torque measurements in subrope tests with and without damage (Mooring rope #1).

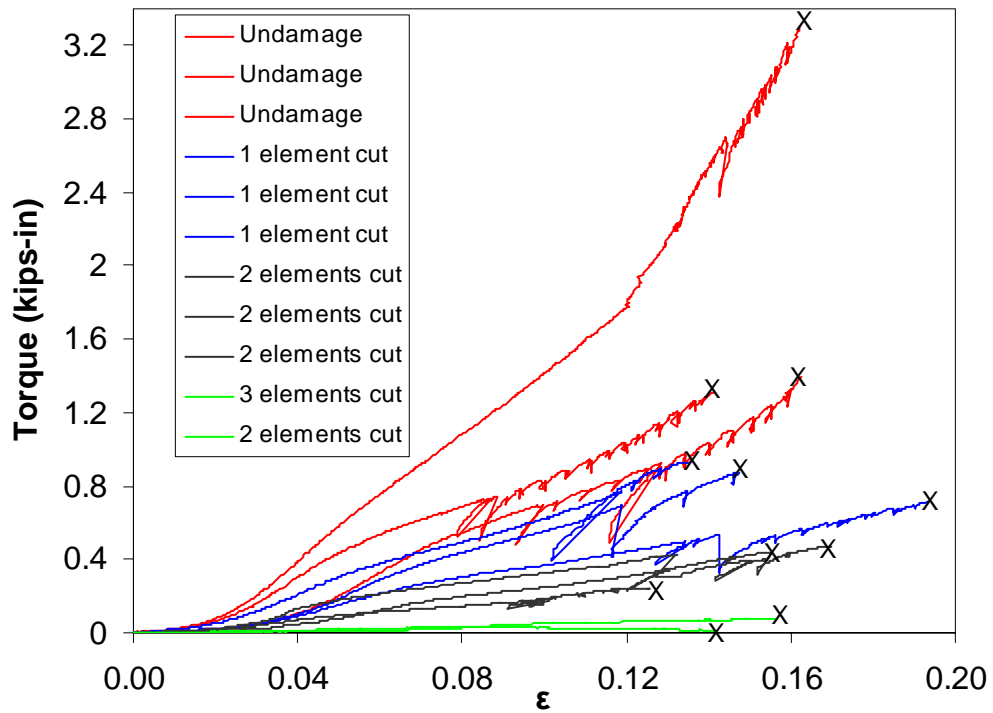


Figure 67 Torque measurements in subrope tests with and without damage (Mooring rope #2).

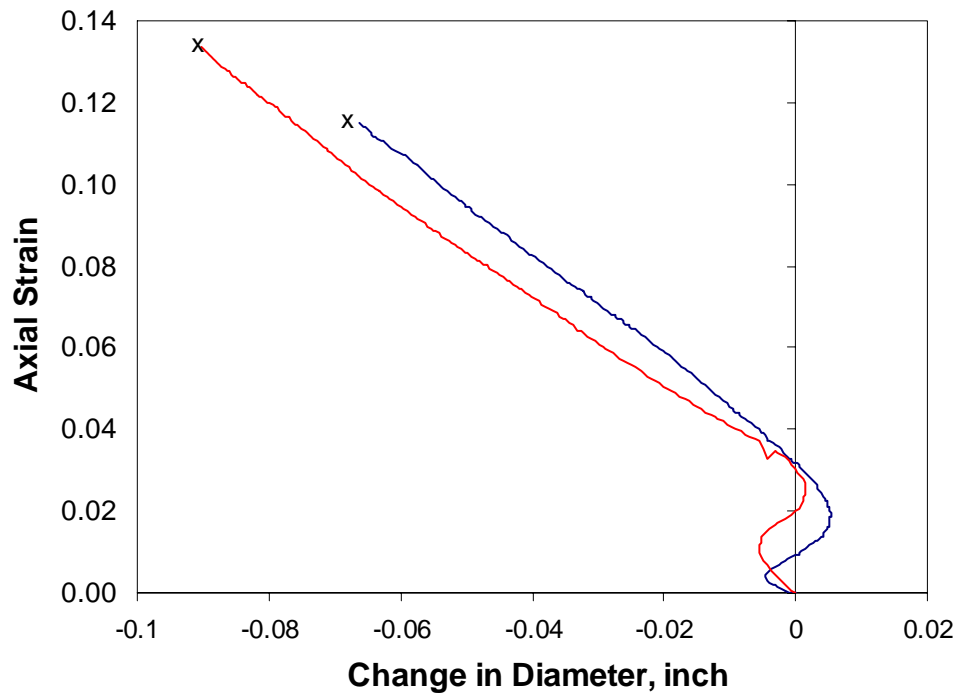


Figure 68 Subrope diameter change as a function of applied axial strain (Mooring rope #1).

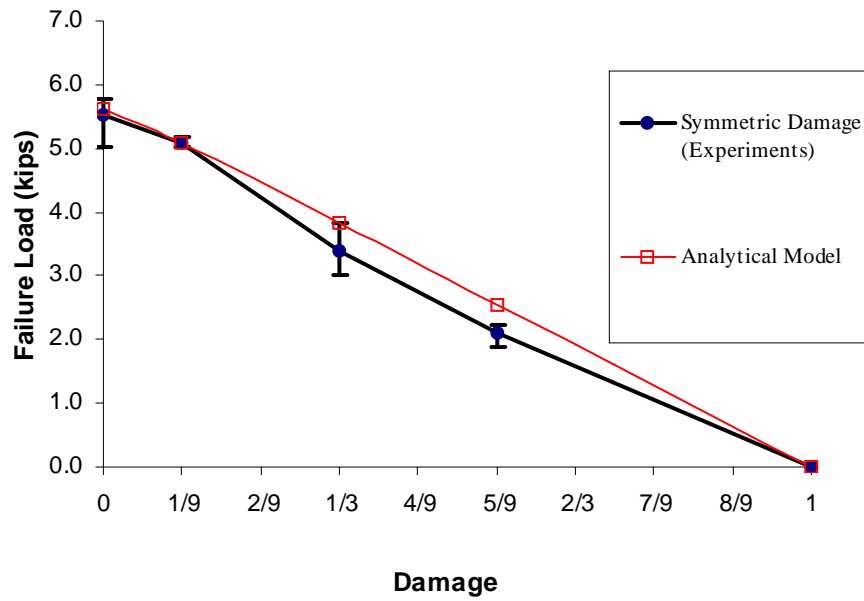


Figure 69 Damaged rope-element failure strength predicted from analytical model and compared with experiment data (Mooring rope #1).